THE MECHANISM OF HEAT TRANSFER IN NUCLEATE POOL BOILING

CHI-YEH HAN
PETER GRIFFITH

March 30, 1962

Contract Nonr-1841 (39)
Report No. 7673-19
Department of Mechanical Engineering
Massachusetts Institute of Technology

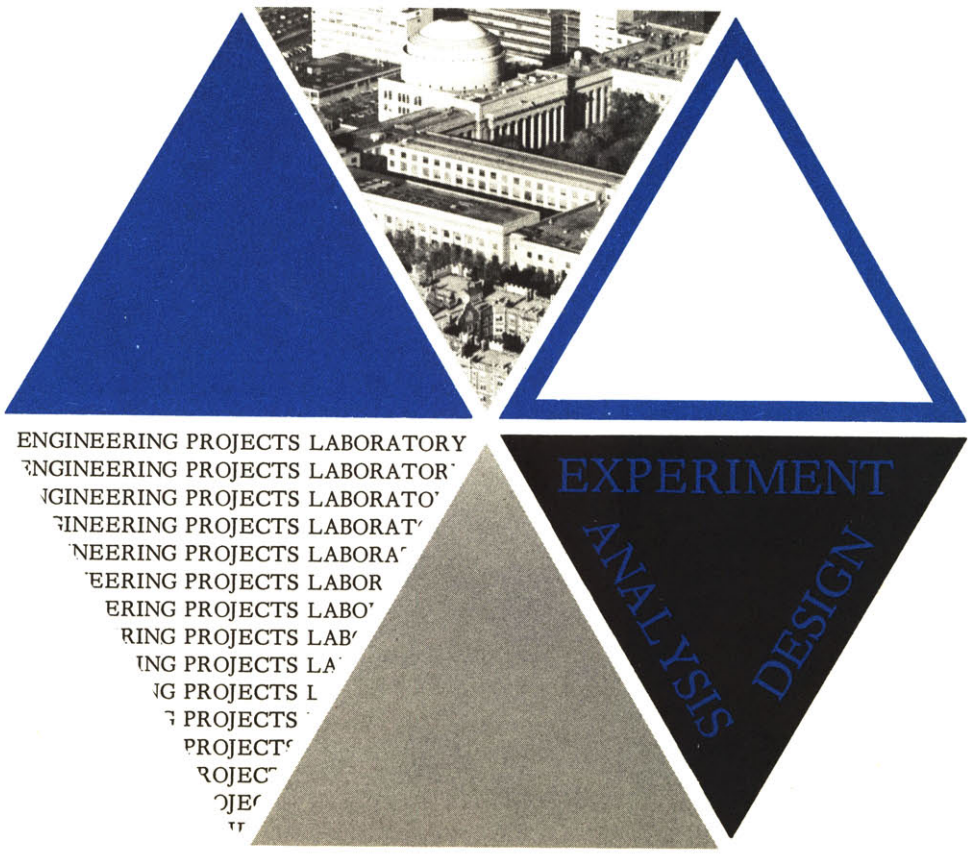

TECHNICAL REPORT NO. 19

THE MECHANISM OF HEAT TRANSFER IN NUCLEATE POOL BOILING

by

Han, Chi-Yeh - Research Assistant
and
Peter Griffith - Associate Professor of Mechanical Engineering

For

THE OFFICE OF NAVAL RESEARCH
NONR - 1841 (39)
DSR No. 7-7673

February 1962

Division of Sponsored Research
Massachusetts Institute of Technology
Cambridge 39, Massachusetts

ABSTRACT

A criterion is developed for bubble initiation from a gas filled cavity on a surface in contact with a superheated layer of liquid. It is found that the temperature of bubble initiation on a given surface is a function of the temperature conditions in the liquid surrounding the cavity as well as the surface properties themselves. It is also found that the delay time between bubbles is a function of the bulk liquid temperature and the wall superheat and is not constant for a given surface.

By consideration of the transient conduction into a layer of liquid on the surface, a thermal layer thickness is obtained. With this thickness and a critical wall superheat relation for the cavity, a bubble growth rate is obtained.

Bubble departure is considered and it is found that the Jakob and Fritz relation works as long as the true (non-equilibrium) bubble contact angle is used. The effect on the departure size of the virtual mass in the surrounding liquid is found to be negligible at one gravity. That is, at one gravity the primary effect of bubble growth velocity on bubble departure size is found to be due to contact angle changes.

The initiation, growth and departure criterions are each experimentally, individually, checked. They are then used to compute the heat transfer near the knee of the boiling curve using only an experimental determination of the number of bubbles as a function of wall superheat and other known quantities. Finally the q vs. $T_w - T_{sat}$ relation is computed and measured and compared. The comparison is satisfactory.

ACKNOWLEDGEMENTS

This work has been entirely supported by the Office of Naval Research and has been performed in the Heat Transfer Laboratory of the Massachusetts Institute of Technology, which is under the direction of Professor W. M. Rohsenow.

We express appreciation for the help and suggestions of Professor W. M. Rohsenow and Professor Moissis throughout the past three years. Thanks are due also to Professor Rightmire and Professor Argon for their suggestions on surface preparation.

TABLE OF CONTENTS

Introduction

When the wall temperature exceeds the saturation temperature of the fluid which is in contact with, a thin layer of superheated fluid near the wall is formed. If there is a cavity on the wall, initially filled with inert gas, a bubble will start to grow from that spot, when the wall superheat becomes sufficiently high. A further increase in the wall superheat will cause an increase in the growth rate and bubble generation frequency.

The growth of the bubble will lift up the superheated liquid layer from heating surface. The departure of the bubble will carry away the thermal layer from an influence circle around the nucleate site. This repeated process gives rise to the high heat transfer in nucleate boiling.

When the bubble frequency exceeds a certain value, the distance between consecutive bubbles is so small that they join together into an unstable and shaky chain and the idealizations made in the analytical portions of this study will no longer be valid for an accurate prediction of the heat transfer rate. Reference (7) gives the boundary dividing the isolated bubble region from the columns of bubbles region. This work, in general applies only to the region of isolated bubbles.

1. Bubble Initiation Theory

a. General Description

A bubble is generally initiated from a small gas filled cavity or crack on a solid surface so long as the surrounding fluid is heated to a sufficiently high temperature. Both the pre-existence of the gas phase and the temperature are necessary but not sufficient. This mechanism has been completely discussed in Reference (3), in the case of homogeneous temperature field. An extension of this mechanism to the non-homogeneous temperature field (which is of primary interest) will be developed in this section. A similar situation can be seen in the process of chicken incubation. A chicken can be incubated from an egg, if and only if, this egg is a fertile one. The bubble initiation mechanism is similar in that, a gas phase must already exist along with the right temperature conditions as shown in Figure 1.

b. Transient Thermal Layer

Since the convection intensity near a solid wall is damped down due to the no slip boundary condition for a solid surface, the use of the pure conduction equation is justified in determining the temperature distribution in this thin layer of fluid near the heating surface. For this particular problem, a simplified physical model is shown in Fig. 2.

Initial condition is

$$\left.\begin{aligned} T &= T_w \quad \text{at} \quad x = 0 \\ T &= T_\infty \quad \text{at} \quad x > 0 \end{aligned}\right\} \; t = 0 \tag{1}$$

Boundary condition is

$$\left.\begin{aligned} T &= T_w \quad \text{at} \quad x = 0 \\ T &= T_\infty \quad \text{at} \quad x = \infty \end{aligned}\right\} \; t > 0 \tag{2}$$

The solution to this problem is found from Ref. (1) as

$$T - T_\infty = (T_w - T_\infty)\, \operatorname{erfc} \frac{x}{2\sqrt{kt}} \tag{3}$$

$$\frac{\partial T}{\partial x} = -\frac{T_w - T_\infty}{\sqrt{\pi k t}}\, e^{-\frac{x^2}{4kt}} \tag{4}$$

at $x = 0$

$$\left(\frac{\partial T}{\partial x}\right)_{x=0} = -\frac{T_w - T_\infty}{\sqrt{\pi k t}} \tag{5}$$

If the actual temperature distribution near the wall is assumed to be a straight line distribution, the slope of this straight line is determined by equation (5). This assumption has been justified through measurements made in Reference (6). With this fact, one can introduce the notion of thickness of transient thermal layer by drawing a tangent line from x = 0 on the $T - T_\infty \sim X$ curve defined by (3), the interception of this straight line on X-axis gives the transient thermal layer thickness as shown in Fig. (3).

$$\delta = \sqrt{\pi k t} \tag{6}$$

This means that the temperature distribution at any instant varies linearly from the wall to $x = \delta$, beyond δ, the fluid does not know whether the wall is hot or cold. The layer thickness increases with the square root of waiting time.

c. Criterion of Bubble Growth Initiation

Having the defintion of the transient thermal layer, one can determine the time required from the beginning of generation of thermal layer to the beginning of bubble growth. This period is defined as the waiting period of a bubble, t_w. The criterion for initiating bubble growth is from Reference (4) that the thermal layer surrounding the bubble nucleus must be at a mean temperature equal to or above the temperature of the vapor in the bubble in order to give rise to an inward flow of heat from the superheated thermal layer to the bubble through the bubble wall. Before bubble growth the bubble is in the condition of thermo-static equilibrium. The equation of static equilibrium for the bubble is then

$$\Delta P = \frac{2\sigma}{R_c} \tag{7}$$

With the help of the Clausius - Clapeyron thermodynamic equilibrium relation, one has

$$\Delta P = \frac{\Delta T}{T_{sat}} \frac{L}{\frac{1}{\rho_v} - \frac{1}{\rho}} \approx \frac{\Delta T \rho_v L}{T_{sat}} \tag{8}$$

where $\Delta T = T_b - T_{sat}$

$\Delta P = P_b - P_{sat}$

T_b, P_b are temperature and pressure of the vapor in the bubble at the initial stage of bubble growth.

Eliminating ΔP from above equations yields

$$\Delta T = T_b - T_{sat} = \frac{2\sigma T_{sat}}{R_c \rho_v L}$$

or

$$T_b - T_\infty = T_{sat} - T_\infty + \frac{2\sigma T_{sat}}{R_c \rho_v L} \tag{9}$$

During the waiting period, the bubble wall can be treated approximately as an insulated hemi-spherical surface of radius R_c (the temperature distribution in the surface tension layer of the bubble is unknown). Presumably there is tangential conduction in a thin layer around the bubble so that the interface temperature is constant. A physical model of this idealization is shown in Fig. 4.

From potential flow theory and the fluid flow analogy, the potential line in fluid flow is just equivalent to the isothermal line in heat conduction, the distance of an isothermal line passing through the top point of a waiting bubble is $\frac{3}{2} R_c$ distant from heating surface when measured on the straight part of this isothermal line.

Fluid temperature at $X = \frac{3}{2} R_c$ is

$$T_f = (T_w - T_\infty)\left(1 - \frac{\frac{3}{2}R_c}{\delta}\right) + T_\infty = T_w - (T_w - T_\infty)\frac{3R_c}{2\delta} \tag{10}$$

Equating this temperature to the bubble temperature yields the criterion of initiation of a bubble growth from a nucleate site of cavity radius R_c as

$$T_{sat} + \frac{2\sigma T_{sat}}{R_c \rho_v L} = T_w - (T_w - T_\infty)\frac{3R_c}{2\delta}$$

or

$$\delta = \frac{3}{2} \frac{(T_w - T_\infty) R_c}{T_w - T_{sat}\left(1 - \frac{2\sigma}{R_c \rho_v L}\right)} \tag{11}$$

when δ is expressed in terms of the waiting period

$$t_w = \frac{\delta^2}{\pi k} = \frac{9}{4\pi k}\left[\frac{(T_w - T_\infty) R_c}{T_w - T_{sat}\left(1 + \frac{2\sigma}{R_c \rho_v L}\right)}\right]^2 \qquad (12)$$

d. The Most Favorable Cavity Radius for Initiating Bubble Growth and the Minimum Waiting Period

As the waiting time increases, the thermal layer increaes until to a certain condition such that the temperature line of luid becomes tangent to the bubble temperature curve. At this instant, if and only if, there is a dry cavity of radius R_{cf} on the heating surface, a bubble will begin to grow from this spot. This radius corresponding to a minimum waiting period, is called the most favorable cavity radius R_{cf}. Let us now turn our attention to the solution of equation (11).

Solving for R_c from (11) yields

$$R_c = \frac{\delta(T_w - T_{sat})}{3(T_w - T_\infty)}\left[1 \pm \sqrt{1 - \frac{12(T_w - T_\infty) T_{sat}\sigma}{(T_w - T_{sat})^2 \delta \rho_v L}}\right] \qquad (13)$$

For any given waiting period, there are two possible cavity radii which will nucleate. When these two cavity radii are equal, it means the two intersecting points coincide, (see Fig. 5), or the fluid temperature line and bubble temperature curve are tangent to each other. Observing (13) gives the condition of equal roots of R_c as

$$1 - \frac{12(T_w - T_\infty) T_{sat}\sigma}{(T_w - T_{sat})^2 \delta \rho_v L} = 0$$

Solving for δ which is by definition δ_{min}, yields

$$\delta_{min} = \frac{12(T_w - T_\infty) T_{sat}\sigma}{\rho_v L (T_w - T_{sat})^2} \qquad (14)$$

Equal root condition in (13) with help of (14) gives

$$R_{cf} = \frac{\delta_{min}(T_w - T_{sat})}{3(T_w - T_\infty)} = \frac{4 T_{sat}}{T_w - T_{sat}} \frac{\sigma}{\rho_v L} \quad (a)$$

$$(t_w)_{min} = \frac{\delta_{min}^2}{\pi k} = \frac{144 (T_w - T_\infty)^2 T_{sat}^2 \sigma^2}{\pi k \rho_v^2 L^2 (T_w - T_{sat})^4} \quad (b) \qquad (15)$$

e. Upper and Lower Bounds of Radius of Active Nucleate Cavity

The thermal layer cannot, in general, increase without limit with the waiting time. It will be washed off by the natural convection of the fluid as it grows beyond the thickness of natural convection layer δ_{NC} . This means

$$\delta_{max} = \delta_{NC} \tag{16}$$

Knowing δ_{max} from the natural convection information, the maximum and minimum cavity radius for initiating a bubble growth can be calculated from (13) with help of (16)

$$(R_c)_{max;\,min.} = \frac{\delta_{NC}(T_w - T_{sat})}{3\,(T_w - T_\infty)}\left[1 \pm \sqrt{1 - \frac{12(T_w - T_\infty)\,T_{sat}\,\sigma}{(T_w - T_{sat})^2 \delta_{NC} \rho_v L}}\,\right] \tag{17}$$

Any cavity outside this interval cannot qualify as an active nucleation site. A diagram is shown in Fig. 5.

f. A Numerical Example for a Quantitative Illustration

Fluid = degased, distilled water

T_{sat} = 212° F = 672° R

T_∞ = 202° F

T_w = 242° F

σ = 38.3 10^{-4} lb./ft.

ρ_v = 0.0374 lbm/ ft.^{3}

k = 1.82 10^{-6} ft.^{2}/sec.

L = 755. 10^3 ft. lb./ lbm.

The most favorable cavity radius for initiating a bubble growth is from (15) a

$$R_{cf} = \frac{4\sigma T_{sat}}{\rho_v L (T_w - T_{sat})} = 1.21 \cdot 10^{-5}\ ft$$

The corresponding thermal layer thickness is from (14)

$$\delta_{min} = \frac{12\,\sigma\,T_{sat}\,(T_w - T_\infty)}{\rho_v L\,(T_w - T_{sat})^2} = 4.89 \cdot 10^{-5}\ ft$$

The minimum waiting period for this bubble is

$$(t_w)_{min} = \frac{\delta_{min}^2}{\pi k} = 4.14 \cdot 10^{-4}\ Sec.$$

2. Bubble Growth Theory

a. Assumptions

i, Neglect any convection, not due to bubble itself, completely.

ii, Neglect the change of mass of fluid due to evaporation or condensation through the interface of vapor and liquid.

iii, One dimensional case is converted into the three dimensional case by the introduction of a curvature factor.

iv, Neglect the inertia force and the surface tension of the fluid.

v, Constant properties of fluid.

vi, Spherical bubble surface.

vii, Uniform wall temperature, mainfluid temperature and fluid pressure.

After a waiting period t_w, the bubble is going to grow. For the first few moments, the surface tension effects and the inertia effects of surrounding fluid are so large such that the growth rate is controlled by momentum equation but after the radius increases to about twice its initial value, the surface tension and inertia effects will become negligible, so that the growth rate is controlled only by the heat transfer. In this study, only the heat transfer effects will be considered for the evaluation of bubble growth curve.

b. Formulation and Solution

For simplicity, the one dimensional physical model for heat transfer mechanism is given in Fig. 6.

Initial condition is

$$\left.\begin{array}{ll} T = T_w - (T_w - T_\infty)\frac{x}{\delta} & \text{for } 0 < x < \delta \\ \text{where } \delta = \sqrt{\pi k t_w} & \\ T = T_\infty & \text{for } \delta < x < \infty \end{array}\right\} t = 0 \qquad (18)$$

Boundary condition is

$$\left.\begin{array}{ll} T = T_{sat} & \text{for } x = 0 \\ T = T_\infty & \text{for } x = \infty \end{array}\right\} t > 0 \qquad (19)$$

Introducing a new variable

$\theta = T - T_{sat}$ such that

$$\theta_{sat} = 0, \quad \theta_w = T_w - T_{sat}, \quad \theta_\infty = T_\infty - T_{sat} \tag{20}$$

then (18) and (19) are transformed to

$$\left.\begin{aligned} \theta &= T_w - T_{sat} - \frac{T_w - T_\infty}{\delta} x = \theta_w - \frac{\theta_w - \theta_\infty}{\delta} x \quad \text{for } 0 < x < \delta \\ \theta &= T_\infty - T_{sat} = \theta_\infty \qquad\qquad \text{for } \delta < x < \infty \end{aligned}\right\} t = 0 \tag{21}$$

&

$$\left.\begin{aligned} \theta &= 0 \quad \text{for } x = 0 \\ \theta &= T_\infty - T_{sat} = \theta_\infty \quad \text{for } x = \infty \end{aligned}\right\} t > 0 \tag{22}$$

The governing equation is then

$$\frac{\partial^2 \theta}{\partial x^2} = \frac{1}{k} \frac{\partial \theta}{\partial t} \tag{23}$$

The problem is now reduced to a semi-infinite conductor, with a prescribed initial temperature $\theta(x, 0) = f(x)$ and surface temperature zero, then the solution of (23) with conditions (21) and (22) will be, from Reference (1)

$$\theta = \frac{1}{2\sqrt{\pi k t}} \int_0^\infty f(x') \left\{ e^{-\frac{(x-x')^2}{4kt}} - e^{-\frac{(x+x')^2}{4kt}} \right\} dx' \tag{24}$$

where

$$\begin{aligned} f(x') &= \theta_w - \frac{\theta_w - \theta_\infty}{\delta} x' \quad \text{for } 0 < x' < \delta \\ &= \theta_\infty \qquad\qquad\qquad\quad \text{for } \delta < x' < \infty \end{aligned}$$

$$\frac{\partial \theta}{\partial x} = \frac{-1}{4\sqrt{\pi}(kt)^{\frac{3}{2}}} \int_0^\infty f(x') \left[(x - x') e^{-\frac{(x-x')^2}{4kt}} - (x + x') e^{-\frac{(x+x')^2}{4kt}} \right] dx' \tag{25}$$

at $x = 0$ (25) becomes

$$\left(\frac{\partial \theta}{\partial x}\right)_{x=0} = \frac{1}{4\sqrt{\pi}(kt)^{\frac{3}{2}}} \int_0^\infty f(x')(2x') e^{-\frac{x'^2}{4kt}} dx'$$

$$= \frac{1}{2\sqrt{\pi}(kt)^{\frac{3}{2}}} \left[\int_0^\delta x' \left(\theta_w - \frac{\theta_w - \theta_\infty}{\delta} x' \right) e^{-\frac{x'^2}{4kt}} dx' + \int_\delta^\infty \theta_\infty x' e^{-\frac{x'^2}{4kt}} dx' \right]$$

$$= \frac{1}{\sqrt{\pi k t}} \left(\theta_w - \frac{\theta_w - \theta_\infty}{\delta} \sqrt{\pi k t}\, \mathrm{erf} \frac{\delta}{\sqrt{4kt}} \right) \tag{26}$$

Referring to the bubble growth model as shown in Fig. 8, the governing equation for bubble growth is

$$\rho_v \left(4\pi R^2 \frac{dR}{dt}\right) \rho_v L = \varphi_c \varphi_s (4\pi R^2) k c \rho \left(\frac{\partial \theta}{\partial x}\right)_{x=0} + \varphi_b (4\pi R^2) \tilde{h}_v (T_w - T_{sat})$$

$$\text{or} \quad \frac{dR}{dt} = \frac{\varphi_c \varphi_s}{\rho_v} \frac{k c \rho}{\rho_v L} \left(\frac{\partial \theta}{\partial x}\right)_{x=0} + \frac{\varphi_b \tilde{h}_v (T_w - T_{sat})}{\rho_v \rho_v L} \qquad (27)$$

where φ_c = curvature factor where $1 < \varphi_c < \sqrt{3}$

φ_s = surface factor $= \dfrac{2\pi R^2 (1+\cos\varphi)}{4\pi R^2} = \dfrac{1+\cos\varphi}{2}$

φ_b = base factor $= \dfrac{\pi R^2 \sin^2\varphi}{4\pi R^2} = \dfrac{\sin^2\varphi}{4}$ (28)

φ_v = volume factor $= \dfrac{\frac{1}{3}(4\pi R^3) - \frac{1}{3}[2\pi R^3 (1-\cos\varphi)] + \frac{1}{3}\pi R^3 \sin\varphi\cos\varphi}{\frac{4\pi R^3}{3}}$

$= \dfrac{2+\cos\varphi(2+\sin^2\varphi)}{4}$

φ = contact angle

$\tilde{h}$ = coefficient of heat transfer from heating surface to the steam bubble through its base area.

Substituting (26) into (27) yields

$$\frac{dR}{dt} = \frac{\varphi_c \varphi_s}{\rho_v} \frac{k c \rho}{\rho_v L} \frac{1}{\sqrt{\pi k t}} \left(\theta_w - \frac{\theta_w - \theta_\infty}{\delta} \sqrt{\pi k t}\, \operatorname{erf} \frac{\delta}{\sqrt{4kt}}\right) + \frac{\varphi_b \tilde{h}_v \theta_w}{\rho_v \rho_v L} \qquad (29)$$

For the case of a bubble growing in an infinite fluid field of superheat θ_w then $\varphi_s = 1$, $\varphi_v = 1$, $\varphi_b = 0$, $\delta = \infty$, and (29) becomes

$$\frac{dR}{dt} = \frac{\varphi_c k c \rho}{\rho_v L} \frac{\theta_w}{\sqrt{\pi k t}} = \frac{\varphi_c}{\sqrt{\pi}} \frac{\theta_w \rho c}{\rho_v L} \sqrt{\frac{k}{t}} \qquad (30)$$

From homogenions solution of bubble growth rate, one has from Scriven's theory (see Reference (18))

$$\frac{dR}{dt} = \sqrt{\frac{3}{\pi}} \frac{\theta_w \rho c}{\rho_v L} \sqrt{\frac{k}{t}} \qquad (31)$$

Comparing (30) and (31), one finds the value of curvature factor to be

$$\varphi_c = \sqrt{3} \qquad \text{for} \quad \varphi = 0 \qquad \delta >> R \qquad (32)$$

Another extreme case is for $\varphi = \pi$, it reduces exactly to one dimensional case then

$$\varphi_c = 1 \tag{33}$$

For $\varphi = 0$, and $\delta \ll \bar{R}$, it reduces to Plesset's thin layer case which gives

$$\varphi_c = \frac{\pi}{2} \tag{34}$$

Combining these three extreme cases, one can manufacture a φ_c such that it satisfies (32), (33), and (34) simultaneously, i.e.,

$$\varphi_c = \left[\sqrt{3} + \frac{\varphi}{\pi}(1-\sqrt{3})\right]\left[(1-\frac{\varphi}{\pi})\frac{\frac{\pi}{2\sqrt{3}}\bar{R}+\delta}{\bar{R}+\delta} + \frac{\varphi}{\pi}\right] \tag{35}$$

where $\bar{R}$ is the time average of bubble radius or

$$\bar{R} \equiv \frac{1}{t}\int_0^t R\,dt \tag{36}$$

Integrating (29), with respect to time t gives

$$R-R_c = \frac{\rho_s \varphi_c}{\rho_v}\frac{k c_p}{\rho_v L}\int_0^t \frac{1}{\sqrt{\pi k t}}\left[\theta_w - (\theta_w-\theta_\infty)\frac{\sqrt{\pi k t}}{\delta}\,\mathrm{erf}\frac{\delta}{\sqrt{4kt}}\right]dt + \frac{\rho_b \tilde{h}\theta_w}{\rho_v \rho_v L}t$$

or

$$R-R_c = \frac{\rho_s \varphi_c}{\rho_v}\frac{k c_p}{\rho_v L}\left[\frac{2\theta_w}{\sqrt{\pi k}}\sqrt{t} - \frac{\theta_w-\theta_\infty}{\delta}\frac{\delta^2}{4k}\left(\frac{4kt}{\delta^2}\,\mathrm{erf}\frac{\delta}{\sqrt{4kt}} + \frac{2}{\sqrt{\pi}}\frac{\sqrt{4kt}}{\delta}e^{-\frac{\delta^2}{4kt}} - 2\,\mathrm{erfc}\frac{\delta}{\sqrt{4kt}}\right)\right] + \frac{\rho_b \tilde{h}\theta_w}{\rho_v \rho_v L}t \tag{37}$$

Normalizing (37) by introducing dimensionless variables

$$\tau = \frac{4kt}{\delta^2} \;\&\; \eta = \frac{R}{\delta} \quad \text{leads to}$$

$$\eta-\eta_c = \frac{\rho_s \varphi_c}{\rho_v}\frac{c_p \theta_w}{\rho_v L}\left[\sqrt{\frac{\tau}{\pi}} - \frac{\theta_w-\theta_\infty}{\theta_w}\left(\tau\,\mathrm{erf}\frac{1}{\sqrt{\tau}} + \frac{2}{\sqrt{\pi}}\sqrt{\tau}\,e^{-\frac{1}{\tau}} - 2\,\mathrm{erfc}\frac{1}{\sqrt{\tau}}\right)\right] + \frac{\rho_b \delta \tilde{h}\theta_w}{4\rho_v \rho_v L k}\tau \tag{38}$$

A bubble growth plot for $T_\infty > T_{sat}$, $T_\infty = T_{sat}$ and $T_\infty < T_{sat}$ in normalized coordinates is shown in Fig. (10).

c. Experimental Result Compared with the Theory

Fluid = Distilled and degased water

k = $1.807\ 10^{-6}$ ft.^{2}/ sec.

c = 1.007 btu/lbm.

ν = $3.16\ 10^{-6}$ ft.^{2}/sec.

γ = 10^{-4} $^1/_{F^\circ}$

σ = $38.3\ 10^{-4}$ lb./ft.

ρ = 59.97 lbm/ft.^{3}

ρ_v = 0.0374 lbm/ ft.^{3}

L = $755\ 10^3$ ft. lb./lbm

P = 1 atm

Surface = 16 k gold polished on clothe wheel by No. 8 diamond compound

φ = 0.750 radian

Data recorded -

T_w = 229.98° F

T_∞ = 205.02° F

T_{sat} = 212° F

Bubble number 1 =

Camera speed = 1140 frames / sec.

t_w = 0.0245 sec.

t_d = 0.0166 sec.

R_d = $0.397 \cdot 10^{-2}$ ft.

δ = $0.372 \cdot 10^{-3}$ ft. (from (6))

R_c = $0.01097 \cdot 10^{-3}$ ft. (from (13))

For $\frac{\rho_s \rho_c}{\rho_v}$ = 1.52

t = $5 \cdot 10^{-3}$ sec.	R = $3.36 \cdot 10^{-3}$ ft.	From (37) with $\tilde{h}_v = 0$
$10 \cdot 10^{-3}$ sec.	$3.89 \cdot 10^{-3}$ ft.	
$15 \cdot 10^{-3}$ sec.	$4.03 \cdot 10^{-3}$ ft.	

Bubble number 2 =

Camera speed = 1260 frames/sec

t_w = 0.0437 sec.

t_d = 0.0167 sec.

R_d = 0.533 · 10^{-2} ft.

δ = 0.498 · 10^{-3} ft. (from (6))

For $\frac{\rho_s \rho_c}{\rho_v}$ = 1.62

t =	5 · 10^{-3} sec.	R = 3.99 · 10^{-3} ft.	From (37)
	10 · 10^{-3} sec.	4.93 · 10^{-3} ft.	with $\tilde{h}_v$ = 0
	15 · 10^{-3} sec.	5.25 · 10^{-3} ft.	

Bubble number 3 =

Camera speed = 1380 frame /sec.

t_w = 0.0275 sec.

t_d = 0.0145 sec.

R_d = 0.479 · 10^{-2} ft.

δ = 0.395 · 10^{-3} ft.

For $\frac{\rho_s \rho_c}{\rho_v}$ = 1.73

t =	5 · 10^{-3} sec.	R = 3.928 · 10^{-3} ft.	From (37)
	10 · 10^{-3} sec.	4.619 · 10^{-3} ft.	with $\tilde{h}_v$ = 0
	15 · 10^{-3} sec.	4.848 · 10^{-3} ft.	

The corresponding bubble growth curves with a comparison from theoretical ones are shown in Fig. 11. The bubble growth history for these three bubbles are shown in Fig. 12, 13, and 14.

d. Discussion of the Bubble Growth Theory

In the bubble growth theory, the thermal layer on the bubble surface is assumed to be picked up by a growth of bubble immediately at the last moment of waiting period. From the high speed photographic study described above, one can see that at the first moments, the bubble growth rate is very high

and the bubble expands laterally at such a rate that in fact a very large piece of thermal layer is picked up during the first few moments. This fact will give a strong support of the one dimensional approach. Actually the bubble growth history is composed of three periods, namely the waiting period t_w , the unbinding period t_{ub} , and the departure period t_d . When the wall superheat increases, the waiting period of bubble at a particular cavity decreases very rapidly. If the thermal layer thickness calculation is still based on the waiting period, the error will be very large. This will make the deviation between the theoretical bubble growth rate and actual one, very large. From Fig. 15, in which the dynamic effect and surface tension effects to bubble growth are shown, the following can be seen: During the waiting period, the bubble is heated in order to initiate growth from its cavity. During unbinding period, the bubble is trying to librate itself from the binding force of surface tension and the inertia effects of its surrounding fluid. The bubble radius increases very slowly and the momentum equation governs the motion of bubble surface. During the departure period, the effects of surface tension and inertia of fluid become so small that the heat transfer equation governs the motion of bubble surface and the thermal layer is picked up by the growing bubble immediately during the first few moments of this period. Therefore the thermal layer thickness for very high wall super heat case where the waiting period is very short should be calculated by

$$\delta = \sqrt{\pi k (t_w + t_{ub})} \quad \text{instead of} \quad \delta = \sqrt{\pi k t_w} .$$

Observations from those 22 bubbles listed in subsection 2-c show that the departure period was nearly constant, the waiting period changed by a factor eight to one. The uneven heating due to a 500 watt light source for photography purpose at the rear side of test section caused a pronounced unsymmet-

rical turbulent convection of fluid which changed the thermal layer distribution. The temperature fluctuations associated with the turbulence gave rise to fluctuations in the waiting period also.

3. Departure Criterion

a. Formulation

From the bubble growth equation and the normalized bubble growth diagram in Fig. 10, one can see that a bubble can either depart from its nucleate site, stay there or collapse there. For the case of $T_\infty > T_{sat}$, the ubble grows monotonically, the bubble must eventually depart from the heating surface due to monotonically increasing buoyant force of the bubble. For the case of $T_\infty \leqq T_{sat}$, it is not clear, one needs a criterion for judging if or not a bubble will depart from the heating surface. In case where the bubble departs, the time to departure is the quantity of interest. This is the next question to be considered.

In order to study the dynamical departure criterion of a bubble from a heating surface, a force and motion analysis is necessary. The assumption of a perfectly spherical bubble will give no information. For this reason, one needs to modify the physical model of bubble from a spherical one to some other shape. In this section, the inertia force effect of the surrounding fluid is calculated by truncated spherical bubble model which is of course not exact. After writing down the governing equations, having chosen the dominating variables of the quasi-static solution which is compatible with the analytical solution in the static case, the assumption of a spherical bubble for evaluating bubble volume and surface is resumed.

From potential flow theory, the inertia mass of the surrounding fluid of a solid sphere departing from a solid plane boundary is (Reference 2)

$$M_1 \approx \frac{91}{128} \rho V$$

By the fact of non-sphericity of the bubble shape and with support of experiments, Davidson had corrected this value to

$$M_1 = \frac{11}{16}\rho\mathcal{V} \tag{39}$$

where $\mathcal{V}$ is the volume of bubble, ρ is the density of the fluid.

M_1 is assumed to be uniformly distributed as a very thin mass layer on the surface of the bubble. Considering the bubble as a thin shell loaded with hydrostatic force and inertia force, defining $p_{x,z}$ as the pressure on the inner face of surface tension layer of the bubble and $P_{x,z}$ as the pressure on the outer face surface tension layer of the bubble, and with the concept of inertia mass layer, one has by momentum equation from Fig. 16.

$$P_{0,0} = P_{\infty,z_0} - \rho g z_0 + \frac{d}{dt}\left(\frac{\frac{11}{16}\rho\mathcal{V}}{S}\frac{dz_0}{dt}\right) \tag{40}$$

$$P_{x,z} = P_{\infty,z} - \rho g(z_0 - z) + \frac{d}{dt}\left\{\frac{\frac{11}{16}\rho\mathcal{V}}{S}\frac{d}{dx}\left[x\sin\varphi - (z_0 - z)\cos\varphi\right]\right\} \tag{41}$$

$$p_{x,z} = p_{0,0} + \rho_v g z \tag{42}$$

Shell formula of force equilibrium applied at the top point of the bubble gives

$$-(P_{0,0} - p_{0,0}) = \frac{\sigma}{b} + \frac{\sigma}{b} = \frac{2\sigma}{b} \tag{43}$$

at point (x , z), it becomes

$$-(P_{x,z} - p_{x,z}) = \frac{\sigma}{\frac{x}{\sin\varphi}} + \frac{\sigma}{\tilde{R}} \tag{44}$$

Defining the equation of meridian curve of the bubble as

$$z = z(x, b, t) \tag{45}$$

where b is a function of time, then

$$\tilde{R} = \frac{1 + \left(\frac{dz}{dx}\right)^2}{\frac{d^2z}{dx^2}}, \quad \sin\varphi = \frac{\frac{dz}{dx}}{\left[1 + \left(\frac{dz}{dx}\right)^2\right]^{\frac{1}{2}}} \tag{46}$$

Substituting (40), (41), and (42) into (43) and (44) and eliminating P's and p's yields

$$\frac{2\sigma}{b} - \frac{\sigma \sin\varphi}{x} - \frac{\sigma}{\tilde{R}} = (P_{x,z} - P_{o,o}) - (P_{x,z} - P_{o,o})$$

$$= (\rho - \rho_v) g z + \frac{d}{dt}\left\{ \frac{11}{16} \frac{\rho v}{S} \frac{d}{dt} [x \sin\varphi - (z_o - z)\cos\varphi - z_o] \right\} \quad (47)$$

Using an approximation

$$v = \frac{4\pi}{3} R^3 ; \qquad S = 4\pi R^2 \quad (48)$$

in which R is determined by (37) and is function of time substituting (46) into (47), the differential equation for the bubble surface can be found.

The initial conditions are that

$$at \quad t = o , \quad b = R_c , \quad z = R_c - \sqrt{R_c^2 - x^2} \quad (49)$$

A numerical method similar to the technical of Bashforth and Adams in Reference 13 is necessary for a complete solution.

putting $x = x_o$, $z = z_o$ into (47) leads to

$$\frac{2\sigma}{b} - \frac{\sigma \sin\varphi_o}{x_o} - \frac{\sigma}{\tilde{R}_o} = (\rho - \rho_v) g z_o + \frac{d}{dt}\left\{ \frac{11}{16} \frac{\rho v}{S} \left[\frac{d}{dt} (x_o \sin\varphi_o - z_o) \right] \right\} \quad (50)$$

where φ_o = angle of contact

Therefore from solution of (47), putting $\varphi = \varphi_o$, one has

$$z_o = z_o (x_o, b, t) \quad (51)$$

where x_o and b are functions of time

or $x_o = x_o (z_o, b, t)$ (52)

Then the departure criterion is

$$x_o = o \qquad z_o > o \quad (53)$$

from which the departure time can be solved by

$$x_o [z_o(t), b(t), t] = o \quad (54)$$

If (54) has no real positive root t_d, it means no departure. If (54) has a real positive root t_d and $z_o(t_d) > o$, it means that the bubble will depart at t_d. This is a complete description of formulation and method for finding out an exact solution.

b. Solution

An approximate solution for this problem can be obtained in the following way.

For case of very small contact angle $\varphi_0 << \frac{\pi}{2}$, (50) can be simplified by assuming a nearly spherical bubble and $x_0 \sin\varphi_0$ negligible compared with z_0 in the last term of (50).

$$\frac{2\sigma}{b} - \frac{\sigma \sin\varphi_0}{x_0} - \frac{\sigma}{\tilde{R}_0} = (\rho - \rho_v) g z_0 \left[1 - \frac{11}{48} \frac{\rho}{(\rho-\rho_v) g R} (\dot{R}^2 + R\ddot{R})\right] \quad (55)$$

The law of motion with help of the notion of the inertia mass layer gives

$$(\rho - \rho_v) V g = \frac{d}{dt}\left(\frac{11}{16} \rho V \frac{1}{2} \frac{dz_0}{dt}\right) - (p_{x_0, z_0} - P) \pi x_0^2 + 2\pi x_0 \sigma \sin\varphi_0$$

With help of (44) and (41), the above equation is reduced to

$$(\rho - \rho_v) V g = \frac{d}{dt}\left(\frac{11}{32} \rho V \frac{dz_0}{dt}\right) - \left(\frac{\sigma \sin\varphi_0}{x_0} + \frac{\sigma}{\tilde{R}_0}\right) \pi x_0^2 + 2\pi x_0 \sigma \sin\varphi_0$$

or $$(\rho - \rho_v) V g = \frac{d}{dt}\left(\frac{11}{32} \rho V \frac{dz_0}{dt}\right) + \pi x_0^2 \left(\frac{\sigma \sin\varphi_0}{x_0} - \frac{\sigma}{\tilde{R}_0}\right)$$

Adding a term $-\frac{11\rho}{48R}(\dot{R}^2 + R\ddot{R}) V$ on both sides of above equation gives

$$(\rho - \rho_v) g V \left[1 - \frac{11}{48} \frac{\rho}{(\rho-\rho_v) g R} (\dot{R}^2 + R\ddot{R})\right] = \pi x_0^2 \left(\frac{\sigma \sin\varphi_0}{x_0} - \frac{\sigma}{\tilde{R}_0}\right)$$
$$+ \frac{d}{dt}\left(\frac{11}{32} \rho V \frac{dz_0}{dt}\right) - \frac{11\rho}{48R} (\dot{R}^2 + R\ddot{R}) V$$

For small contact angle φ_0, $z_0 \approx 2R$, $V \approx \frac{4\pi}{3} R^3$, one has then

$$(\rho - \rho_v) g V \left[1 - \frac{11}{48} \frac{\rho}{(\rho-\rho_v) g R} (\dot{R}^2 + R\ddot{R})\right] = \pi x_0^2 \left(\frac{\sigma \sin\varphi_0}{x_0} - \frac{\sigma}{\tilde{R}_0}\right) + \frac{11\pi\rho R^2}{18} (4\dot{R}^2 + R\ddot{R}) \quad (56)$$

Now dropping out all subscripts 0 in (55) and (56) and keeping their original definitions yields

$$\left.\begin{aligned} &\frac{1}{\tilde{R}} + \frac{\sigma \sin\varphi}{x} = \frac{2}{b} - \frac{(\rho-\rho_v) g z}{\sigma} \left[1 - \frac{11\rho}{48(\rho-\rho_v) g R} (\dot{R}^2 + R\ddot{R})\right] \\ &(\rho - \rho_v) g V \left[1 - \frac{11\rho}{48(\rho-\rho_v) g R} (\dot{R}^2 + R\ddot{R})\right] \\ &\quad = \pi x^2 \left(\frac{\sigma \sin\varphi}{x} - \frac{\sigma}{\tilde{R}}\right) + \frac{11\pi R^2}{48} (4\dot{R}^2 + R\ddot{R}) \end{aligned}\right\} \quad (57)$$

For the static case $\frac{d}{dt} \equiv 0$, all dot and double dot terms in (57) drop out, so (57) is reduced to

$$\left.\begin{aligned} &\frac{1}{\tilde{R}} + \frac{\sigma \sin\varphi}{x} = \frac{z}{b} - \frac{(\rho - \rho_v) g z}{\sigma} && \text{(a)} \\ &\vartheta = \frac{\pi x^2 \sigma}{(\rho - \rho_v) g} \left(\frac{\sin\varphi}{x} - \frac{1}{\tilde{R}} \right) && \text{(b)} \end{aligned}\right\} \quad (58)$$

The departure criterion for the governing equation (58) was given in Reference (9) by Fritz. He used the numerical analysis result of Bashforth and Adams (Reference 13) to correlate the dimensionless quantity $\frac{\vartheta_{max}}{a_s^3}$ against the the contact angle. He concluded that the bubble will depart at maximum volume, so that

$$\vartheta_{max} = \left[\frac{\pi x^2 \sigma}{(\rho - \rho_v) g} \left(\frac{\sin\varphi}{x} - \frac{1}{\tilde{R}} \right) \right]_{departure} = 0.313\, a_s^3 \varphi^3 \quad (59)$$

where

$$a_s = \sqrt{\frac{2\sigma}{g(\rho - \rho_v)}} \quad (60)$$

which is called Laplacian characterizing length of a static bubble (59) is supported successfully by experiments for $\varphi = 0$ up to $\varphi = 2.4$ radians.

Comparing (57) and (58) term by term, one can see that a quasi-static solution exists, if the static Laplacian length a_s is replaced by a dynamic length such that

$$a_d = a_s \left[1 - \frac{11\rho}{48(\rho - \rho_v) g R} (\dot{R}^2 + R\ddot{R}) \right]^{-\frac{1}{2}} \quad (61)$$

then the quasi-static criterion for dynamic departure will be

$$\vartheta_{max} \geqq \left[0.313\, a_d^3 \tilde{\varphi}^3 + \frac{11\pi\rho R^2 (4\dot{R}^2 + R\ddot{R})}{18} \frac{a_d^2}{2\sigma} \right]_{departure}$$

or

$$\vartheta_{max} \geq \left[\frac{0.313\, a_d^3 \tilde{\varphi}^3}{1 - \frac{11\rho}{24R} (4\dot{R}^2 + R\ddot{R}) \frac{a_d^2}{2\sigma}} \right]_{departure} \quad (62)$$

where $\tilde{\varphi}$ is the dynamic contact angle.

This departure criterion is based on an assumption which gives the right result in the static case and yields an estimate of the effect of dynamic forces on the departure size of that bubble.

Crudely one can regard the dynamic forces as altering the gravity that the bubble sees. Observations from the high speed photographs of bubbles show that the contact angle apparently changes with the velocity of the triple interface. It is experimentally well established that the contact angle only has its equilibrium value when the system is static. In our experiments (see Fig. 12, 13 and 14) the change in the contact angle was obvious as the bubble went from advancing to receding and also when the rate of growth changed. The departure size was found to be a function of the receding dynamic contact angle rather than the mean value experienced by the bubble which is in contact with the surface. The most important force change, the contact angle, appears to be the viscous force. To a first approximation, the change in contact angle might be linear in the ratio of the viscosity force and surface tension force. Dividing bubble Weber number with bubble Reynolds number yields a new number,

$$\left(\frac{\rho \dot{R}^2 R}{\sigma}\right) \Big/ \left(\frac{\dot{R} R}{\nu}\right) = \frac{\rho \dot{R} \nu}{\sigma} \tag{63}$$

which is the ratio of viscosity force to the surface tension force. (See the appendix)

The correlation relating $\tilde{\varphi}$ to φ is then

$$\tilde{\varphi} = (1 + \Lambda \frac{\rho \dot{R} \nu}{\sigma}) \varphi \tag{64}$$

where Λ is a constant to be determined by experiments. In Reference (10), Staniszewski had performed 51 experiments using water and alcohol as the fluids at different system pressure, Λ can be evaluated using these experiments and is

$$\Lambda = 6850 \tag{65}$$

Actual measurements of the dynamic contact angle from Figs. 12, 13 and 14, show that (65) was in good agreement.

Since Staniszewski's experiments were done at relatively low wall superheat, the dynamical effects other than the contact angle change are secondary to the gravity effects on departure.

This, we feel, is the primary cause of apparent dynamic effect on departure size by Staniszewski. The value of contact angle reported by Staniszewski are actually averages for a large number of readings. It is assumed here, on the basis of our own observations, that the dependence of the departure size on the bubble growth rate is a result of a change in contact angle due to dynamic effects rather than any dynamic effects. In the subsequent subsection, a calculation will be made to show that the dynamic effects in the liquid are, indeed negligible for the condition under which our data and that of Staniszewski's were taken.

(62) is only an approximate criterion for the case of small contact angle. The exact one should be found from (53) which is too complicated to work out for this study as far as the time is concerned. However with the suggestion reported in subsection 3 - a., and a complete understanding of Reference 13, a general departure criterion might be worked out with the help of machine computation.

Putting $g = 0$ in (47), a criterion for zero gravity case can be obtained.

To show the dynamic contact angle effects on bubble departure, Stanizewski's data is shown in Fig. 18 in which

$$\left.\begin{aligned} R_d &= 0.4215\,\varphi\sqrt{\frac{2\sigma}{g(\rho-\rho_v)}}\,(1+10.44\,\dot{R}_d) \\ R_o &= 0.4215\,\varphi\sqrt{\frac{2\sigma}{g(\rho-\rho_v)}} \end{aligned}\right\} \qquad (66)$$

where R_d is in ft.

φ is in radian

$\dot{R}_d$ is in ft./sec.

c. The Period to Departure and the Bubble Generation Frequency

Putting $\mathcal{V} = \frac{4\pi}{3}R^3$ and $R = R_d$, one can solve for R_d from (62). Having solved for R_d, the corresponding time t_d, the departure period, can be solved by (37).

With t_d found from (37) and t_w found from (12) the bubble generating frequency is then

$$f = \frac{1}{t_w + t_d} \tag{67}$$

A bubble generating cycle diagram is shown in Fig. 18.

d. Discussion

In this analysis, the effect of the disturbance of the surrounding fluid due to natural convection is completely discarded. Actually the natural convection of the surrounding fluid, the irregularity of bubble shape, the surface condition of the wall, the disturbances arising from a growth and a departure of the neighboring bubbles, the bubble population density will strongly influence the departure diameter. Therefore, a deviation of only $\pm$ 10% of the departure diameter from the experimental result is not surprising

e. Comparison with Experimental Results

Fluid = Distilled and degased water

Surface = No. 8 diamond compound polished gold surface

φ = 0.750 radian

Data are exactly the same as that in bubble growth theory.

For bubble number 1 -

$*R_d = 4.009 \cdot 10^{-3}$ ft. from (62) and (48)

$R_d = 3.974 \cdot 10^{-3}$ ft. from experiment

For bubble number 2 -

$R_d = 5.363 \cdot 10^{-3}$ ft. from (62) and (48)

$R_d = 5.328 \cdot 10^{-3}$ ft. from experiment

For bubble number 3 -

$R_d = 4.886 \cdot 10^{-3}$ ft. from (62) and (48)

$R_d = 4.792 \cdot 10^{-3}$ ft. from experiment

* The value $\dot{R}$ in $\tilde{\varphi}$ was taken from the slope of experimental bubble growth curve at $t = t_d$ instead of theoretical ones.

A plot of measured departure radii against the calculated ones is shown in Fig. 19.

4. Heat Transfer Correlation

a. Explanation of Boiling Curve

Boiling curve can be best explained by the theory of "bulk convection of the transient thermal layer". Observations show that when the wall temperature exceeds the saturation temperature of the fluid, the heat transfer increases very rapidly with the wall temperature. Many researchers have tried to explain why this occurs. The following study explains these observations by means of a so-called theory of bulk convection of the transient thermallayer, or simply bulk convection theory. When the boiling starts, the bubbles depart from the heating surface. In departing, the bubbles bring part of the layer of superheated liquid adjoining the bubble into the main body of fluid. At the same time, the cold fluid flows onto the heating surface. The heat transfer rate for the first few moments after this process is very high due to the very high temperature gradient near the wall. After a certain time, a new thermal layer is built-up, and a new bubble starts to grow. When this bubble grows to a certain size, it departs from the heating surface and a new thermal layer is brought to the main body of fluid again. By this kind of repeated transportation of thermal layer (which is technically called bulk convection), heat is transferred to the fluid from the wall. The heat transfer rate by this process is nearly proportional to the square root of bubble generation frequency. In Fig. 20, one can see that from A to B, heat transfer rate increases very rapidly due to the increase in $T_w - T_{sat}$ which increases the bubble generating frequency, the enthalpy content of the transient thermal layer and the density of active cavity population. At B the active cavity population has been increased to a saturation state such that the influence circle of each bubble touches one another. A further increase of $T_w - T_{sat}$ does not increase area of production of transient thermal layer, but the bubble frequency and enthalpy content of thermal layer

continues to increase. Therefore after B the rate of increase of q is reduced. B is a point of inflection. From B to C the bubble frequency increases until to a certain stage such that unstable and shaky vapor jets are formed. These continuous vapor columns reduce the effective area of production of transient thermal layer, such that the curve becomes concave downward. From C to D, the effective area of production of transient thermal layer decreases more rapidly than increase of the enthalpy content in the thermal layer due to increase of $T_w - T_{sat}$, therefore the curve drops. At point D, the effective area of production of transient thermal layer has been reduced to zero, a steady and continuous blanket of vapor exists between the heating surface and main fluid. The fluid gets essentially no chance to touch the heating surface, therefore no transient thermal can be built up on the heating surface and the heat transfer rate reaches to a minimum value. Bulk convection process is completely stopped at D. A further increase of $T_w - T_{sat}$ will increase heat flux again by radiation and conduction across the gap.

b. Mechanism of Heat Transfer

The heating surface in pool boiling is divided into two parts, the bulk convection area and the natural convection area. In the area of bulk convection, heat is assumed to be transferred into the fluid by transient conduction process. Following the departure of a bubble from the heating surface, a piece superheated liquid is brought into the main body of the fluid. By this kind of repeated process heat is transferred from heating surface to the main body of the fluid. In the area of the natural convection, heat is supposed to be transferred from heating surface into the main body of fluid by the usual convection process in a continuous manner. A physical model of bulk convection mechanism is shown in Fig. 21.

At stage 1, a piece of superheated transient thermal layer is torn off from heating surface by the departing bubble, and at the same time, the cold fluid from the main body of the fluid flows onto the heating surface, after a time interval t_w, this cold liquid layer is heated to a condition such that the tiny bubble on that cavity is able to grow which is shown as stage 2. At stage 3, the bubble grows laterally with a very high rate such that a very large piece of thermal layer is picked up in a very short time interval. At stage 4, the bubble is going to depart from the heating surface which will bring the situation immediately to stage 1 again. This cyclic process furnishes a way to transfer the heat from the heating surface to the main body of the fluid.

The system which is used to evaluate the heat transfer per bubble cycle is as follows.

c. Formulation

i, Natural Convection Component

A theoretical study of natural pool convection points out that the natural convection heat transfer can be correlated by using two dimensionless groups namely

The Nusselt Number $Nu = \frac{\tilde{h} D}{\rho c k}$

The Rayleigh Number $Ra = \frac{\gamma g (T_w - T_\infty) D^3}{k \nu}$ (68)

For Laminar Range

$$10^5 < Ra < 2 \cdot 10^7$$
$$Nu = 0.54\, Ra^{\frac{1}{4}} \quad \text{(a)}$$

For Turbulent Range (69)

$$2 \cdot 10^7 < Ra < 3 \cdot 10^{10}$$
$$Nu = 0.14\, Ra^{\frac{1}{3}} \quad \text{(b)}$$

where $D = \sqrt{A}$

A = Area of heating surface.

This correlation was first studied experimentally by cryder and Finalborgo and was summarized by Fishenden and Saunders.

Substituting (68) into (69) and making use of the definition of heat transfer coefficient yield

For Laminar Range

$$10^5 < Ra < 2 \cdot 10^7$$

$$q_{NC} = \tilde{h}(T_w - T_\infty) = 0.54 \rho c \left[\frac{\gamma g (T_w - T_\infty)^5 k^3}{D\nu}\right]^{\frac{1}{4}} \quad (70)$$

For Turbulent Range

$$2 \cdot 10^5 < Ra < 3 \cdot 10^{10}$$

$$q_{NC} = \tilde{h}(T_w - T_\infty) = 0.14 \rho c \left[\frac{\gamma g (T_w - T_\infty)^4 k^2}{\nu}\right]^{\frac{1}{3}} \quad (71)$$

For illustrative purpose, a numerical example is given as follows.

Liquid = water

T_{sat}	$= 212^\circ$ F	ρ	$= 59.97$ lbm/ft.^{3}
T_w	$= 242^\circ$ F	c	$= 1.007$ btu/lbm $^\circ$F
T_∞	$= 202^\circ$ F	g	$= 32.2$ ft./sec.^{2}
D	$= 1\ 7/8'' = 0.156$ ft		
k	$= 1.81 \cdot 10^{-6}$ ft.^{2}/sec.		
γ	$= 10^{-4}$ $^1/^\circ$F		
ν	$= 0.316 \cdot 10^{-5}$ ft^2/sec.		

From (68) $Ra = \dfrac{\gamma g (T_w - T_\infty) D^3}{k\nu} = 8.54 \cdot 10^7 > 2 \cdot 10^7$

which is in turbulent range, from (71)

$$q_{NC} = 0.14 \rho c \left[\frac{\gamma g (T_w - T_\infty)^4 k^2}{\nu}\right]^{\frac{1}{3}} = 1.725 \text{ B.t.u./(ft}^2\text{.sec)}$$

The thickness of the thermal layer of natural convection is

$$\delta_{NC} = \frac{\rho c k}{q_{NC}} (T_w - T_\infty) = 0.254 \cdot 10^{-2} \text{ ft} \quad (72)$$

ii, Bulk Convection Component

From equation (2), one can obtain the heat transferred through unit area of heating surface to the fluid during time t as

$$\int_0^\infty (T - T_\infty) c \rho \, dx = c\rho (T_w - T_\infty) \int_0^\infty \operatorname{erfc} \frac{x}{2\sqrt{kt}} \, dx = \frac{2\rho c (T_w - T_\infty)\delta}{\pi} \quad (73)$$

For this case, δ is not a constant throughout the bubble base where the transient conduction thermal layer is developing. Such a donut-shaped layer is illustrated in Fig. 22.

For convenience in integration, the initial state is taken at the end of waiting period, so that

$$\left.\begin{aligned} \delta &= \sqrt{\pi k (t_w + t)} \\ \delta_c &= \sqrt{\pi k t_w} = \delta_w \\ \delta_d &= \sqrt{\pi k (t_w + t_d)} \end{aligned}\right\} \qquad (74)$$

Making use of (72), the heat transferred into transient thermal layer as well as in the main body of fluid beyond the transient layer during one bubble formation cycle is

$$\begin{aligned} \Delta Q &= \int_{R_c}^{R_d} \frac{2\rho c (T_w - T_\infty)\delta}{\pi} (2\pi r\, dr) + \pi (R_i^2 - R_d^2) \frac{2\rho c (T_w - T_\infty)}{\pi} \delta_d \\ &= \frac{2\rho c (T_w - T_\infty)}{\pi} \left[\int_{R_c}^{R_i} 2\pi r \delta\, dr + \pi (R_i^2 - R_d^2) \delta_d \right] \end{aligned} \qquad (75)$$

where R_i is influence radius

$$\left.\begin{aligned} R_i &= 2 R_d \text{ for the isolated bubble case} \\ R_i &< 2 R_d \text{ for the close packed case} \end{aligned}\right\} \qquad (76)$$

Since $R_c << R_d$, and δ is nearly linear in r, so (75) can be approximated to yield

$$\Delta Q = 2\rho c (T_w - T_\infty) \left[R_i^2 \delta_d - \frac{1}{3} R_d^2 (\delta_d - \delta_c) \right] \qquad (77)$$

If "n" is the number of active cavities of radius R_c per unit area of heating surface, and f is the frequency of bubble generation, then the heat transfer rate per unit area due to bulk convection of the transient thermal layer is approximately from (77)

$$q_{BC} = nf\, \Delta Q = 2\rho c (T_w - T_\infty) nf \left[R_i^2 \delta_d - \frac{1}{3} R_d^2 (\delta_d - \delta_c) \right] \qquad (78)$$

iii, Vapor Convection Component

In addition to the heat transferred directly to fluid, heat is also transferred directly into bubble through the heating

surface exposed to the vapor inside the bubble. This component is important only at very high wall superheat. It can be omitted in nucleate boiling region but must be considered in the film boiling region.

$$q_{vc} \doteq n A_c (T_w - T_{sat}) \tilde{h}_v + n f \tilde{h}_v \int_{R_b}^{R_d \sin\varphi} (t_d - t)(T_w - T_{sat}) 2\pi R_b \, dR_b \quad \cdots\cdots\cdots\cdots\cdots\cdots\cdots\cdots (79)$$

where $R_b \doteq R \sin\varphi$ = base circle radius of bubble

A_c = Surface area of cavity

$\tilde{h}_v$ = Heat transfer coefficient of vapor convection.

Since A_c and R_c are very small quantities, (79) can be reduced roughly to

$$q_{vc} \approx \frac{\pi}{3} n f \tilde{h}_v (T_w - T_{sat}) t_d R_d^2 \sin^2\varphi \qquad (80)$$

iv, General Expression of Heat Transfer

Combining (70) (or (71)), (79) and (80) leads to

$$q = q_{Nc} + q_{Bc} + q_{vc}$$
$$= (1 - \pi n R_i^2) Nu \frac{\rho c k}{D} (T_w - T_\infty) + 2\rho c (T_w - T_\infty) n f \left[R_i^2 \delta_d - \frac{R_d^2}{3}(\delta_d - \delta_c)\right]$$
$$+ \frac{\pi}{3} n f \tilde{h}_v (T_w - T_{sat}) t_d R_d^2 \sin^2\varphi \quad \cdots\cdots (81)$$

A three dimensional sketch of the heat transfer as a function of subcooling and wall superheat is given in Fig. 23 in which the effects of subcooling of main fluid and wall superheat can be easily interpreted by means of the bulk convection theory.

d. Discussion

The population density of bubbles at the close packed condition is such that the bubbles are so densely packed that the influence circle of one nucleate cell touches its neighbors, considering one half cell as indicated in Fig. 24 by shaded area, one has

$$n_{cp} = \frac{N_{cp}}{A} = \frac{\frac{1}{2}}{\frac{1}{2}(2R_i \sqrt{3} R_i)} = \frac{1}{2\sqrt{3} R_i^2} \qquad (82)$$

where $R_i = 2 R_d$ (83)

(83) was justified by some rough experiments in which a ball of radius "a" was pulled up from the bottom of water tank

which has a layer of chalk powder on the bottom. Observations showed that the chalk powder within a circle of radius $R_i \approx 2a$ moved toward the center forming a vortex ring in the wake part of the ball. This vortex ring is a method of scavenging away the thermal layer within this influence circle and putting a new layer of cold liquid on the heating surface bounded by the influence circle. A sketch of this process is shown in Fig. 25.

From potential flow theory, the velocity potential and stream line function in the surrounding fluid of a departing sphere of radius a from a solid plane boundary are from Reference (2)

$$\Phi = -\frac{U}{2}\left(\frac{a^3}{r^3} + \frac{a^3 r}{4h^3} + \frac{a^6 r}{32h^6} + \frac{a^6}{8h^3 r^2} + \frac{a^9}{64h^6 r^2} + \cdots\right)\cos\theta + C_1 \quad (84)$$

$$\Psi = -\frac{U}{4}\left(-\frac{2a^3}{r} + \frac{a^3 r^2}{4h^3} + \frac{a^6 r^2}{32h^6} - \frac{a^6}{4h^3 r} - \frac{a^9}{32h^6 r} + \cdots\right)\sin^2\theta + C_2 \quad (85)$$

The velocity components at point P in radial and meridian directions are

$$v_r = -\frac{\partial \Phi}{\partial r} = \frac{U}{2}\left(-\frac{2a^3}{r^3} + \frac{a^3}{4h^3} + \frac{a^6}{32h^6} - \frac{a^6}{4h^3 r^3} - \frac{a^9}{32h^6 r^3} + \cdots\right)\cos\theta \quad (86)$$

$$v_\theta = \frac{-1}{r}\frac{\partial \Phi}{\partial \theta} = -\frac{U}{2}\left(\frac{a^3}{r^3} + \frac{a^3}{4h^3} + \frac{a^6}{32h^6} + \frac{a^6}{8h^3 r^3} + \frac{a^9}{64h^6 r^3} + \cdots\right)\sin\theta \quad (87)$$

putting $a = R_a$, $h = R_d$ in (86) and (87) gives roughly the velocity components of the fluid surrounding a departing bubble as

$$v_r \doteq \frac{-U}{64}\left(\frac{73 R_a^3}{r^3} - 9\right)\cos\theta + \cdots$$

$$v_\theta \doteq -\frac{U}{64}\left(\frac{73 R_a^3}{2r^3} + 9\right)\sin\theta + \cdots \quad (88)$$

where U is the bubble rising velocity at departure.

Example with experimental data taken from Reference (5).

$q = 8.3 \cdot 10^4$ btu/ft.^{2}/hr. = 23 btu/ft.^{2}/sec.

T_w = 230°F evaluated from bubble growth theory based on the bubble growth curve given in Reference (5).

T_{sat} = 212° F

T_∞ = 196° F

$t_w = 12 \cdot 10^{-3}$ sec.

$t_d = 12 \cdot 10^{-3}$ sec.

$R_d = 0.040$ in $= 0.0033$ ft.

From (74)

$\delta_c = \sqrt{\pi k t_w} = 2.62 \cdot 10^{-4}$ ft

$\delta_d = \sqrt{\pi k (t_w + t_d)} = 3.70 \cdot 10^{-4}$ ft

$f = \frac{1}{t_w + t_d} = 41.6$ cycle/sec.

Fig. 5 in Reference 5 shows that this is the close packed case $R_i = 2 R_d = 0.0066$ ft., (82) gives

$$n = \frac{1}{2\sqrt{3} R_i^2} = 6630 \quad 1/ft^2$$

From (78), the heat transfer due to bulk convection is

$$q_{BC} = 2nf\rho c (T_w - T_\infty) \left[R_i^2 \delta_d - \frac{1}{3} R_d^2 (\delta_d - \delta_c)\right] = 17.3 \text{ B+U}/(ft^2 \cdot sec)$$

which is about 75% of the total heat flux supplied to the heating surface.

The heat flux required for evaporation of vapor into bubble is

$$n f L \vartheta_{max} \rho = 1.51 \quad \text{B+U}/(ft^2 \cdot sec)$$

where $\vartheta_{max} = \frac{4\pi}{3} R_d^3$

which is about 6% of the total heat flux.

The heat transfer due to natural convection for close packed case is from (71) and (82)

$$q_{Nc} = \left(1 - \frac{\pi}{2\sqrt{3}}\right) 0.14 \rho c \left[\frac{\gamma g (T_w - T_\infty)^4 k^2}{\nu}\right]^{\frac{1}{3}} = 0.132 \quad \text{B+U}/(ft^2 \cdot sec)$$

which is about 0.6% of the total heat flux.

Most of the difference between the calculated and experimental results is due to geometric idealization. From above example, one can see that the bulk convection of transient thermal layer from heating surface to the main fluid constitutes a chief means of heat transfer. Bubbling is the only natural mechanical driving force which propels such a bulk convection. The bubble growth theory and the departure criterion in nucleate boiling heat transfer are important not because they can carry a large amount of heat due to evaporation of fluid into the bubble voids (only a few percent), but because they supply the way to take off the transient thermal layer repeatedly from the heating surface.

e. Comparison with Experiment Results

Two sets of experimental results are presented in this section; one set is ours, while the other was taken from Ref. 17, both results were compared with this theory.

i, Result 1 - (From our experiments)

Fluid used: Distilled degased water

Surface: Gold layer plated on copper base, polished with No. 8 diamond compound.

System pressure $P = 1$ atm

Data point 1: $Q_R = 0.0620$ btu/sec. from (91)

$T_w = 218.73^\circ$ F

$T_{sat} = 212.00^\circ$ F

$T_\infty = 178.56^\circ$ F

$N = 12$;

$N_i = 12$ of $R_c = 3.0460 \cdot 10^{-5}$ ft. from (17), $(R_c)_{min}$ was taken as the cavity radius, since $(R_c)_{max}$ is nearly a hundred times larger than the surface texture dimension.

$N_a = 0$

$Q_P = 0.0620$ btu/sec. from (81)

Data point 2 = $Q_R = 0.1202$ btu/sec. from (91)

$T_w = 235.09^\circ$ F

$T_{sat} = 212.00^\circ$ F

$T_\infty = 199.72^\circ$ F

$N = 18$;

$N_a = 12$ of $R_c = 3.0460 \cdot 10^{-5}$ ft.

$f = 69.15$ /sec. from (17), (11), (12), (62), (37), and (67)

$N_i = 6$ of $R_c = 0.7859 \cdot 10^{-5}$ ft.

$R_d = 4.15 \cdot 10^{-3}$ ft. from (62), (37)

$Q_P = 0.1142$ btu/sec. from (81)

Data point 3 = $Q_R = 0.1433$ btu /sec.

$T_w = 237.11^\circ$ F

$T_{sat} = 212^\circ$ F

$T_\infty = 201.87^\circ$ F

$N = 20.$

$N_a = 18.$
- 12 of $R_c = 3.046 \cdot 10^{-5}$ ft., $f = 78.46$ 1/sec.
- 6 of $R_c = 0.7859 \cdot 10^{-5}$ ft., $f = 53.08$ 1/sec.

$N_i = 2$ of $R_c = 0.7240 \cdot 10^{-5}$ ft.

$R_d = 4.215 \cdot 10^{-3}$ ft.

$Q_P = 0.1412$ btu /sec.

Data point 4 = $Q_R = 0.1866$ btu/sec.

$T_w = 237.61^\circ$ F

$T_{sat} = 212^\circ$ F

$T_\infty = 201.38^\circ$ F

$N = 20$

$N_a = 20;$
- 12 of $R_c = 3.046 \cdot 10^{-5}$ ft., $f = 80.72$ 1/sec.
- 6 of $R_c = 0.7859 \cdot 10^{-5}$ ft., $f = 61.56$ 1/sec.
- 2 of $R_c = 0.7240 \cdot 10^{-5}$ ft., $f = 6.44$ 1/sec.

$N_i = 0$

$R_d = 4.231 \cdot 10^{-3}$ ft.

$Q_P = 0.1584$ btu/sec.

Data point 5 = $Q_R = 0.2157$ btu/sec.

$T_w = 240.65^\circ$ F

$T_{sat} = 212.00^\circ$ F

$T_\infty = 200.53^\circ$ F

$N = 20$;

$N_a = 20$:
- 12 of $R_c = 3.046 \cdot 10^{-5}$ ft., $f = 88.03$ 1/sec.
- 6 of $R_c = 0.7859 \cdot 10^{-5}$ ft., $f = 87.06$ 1/sec.
- 2 of $R_c = 0.7240 \cdot 10^{-5}$ ft., $f = 78.60$ 1/sec.

$N_i = 0$

$R_d = 4.322 \cdot 10^{-3}$ ft.

$Q_P = 0.2056$ btu /sec.

A comparison of experimental result with theoretical ones is shown in Fig. 26.

ii, Result 2 - (From Fig. 8 on Reference (17))

Fluid: n - pentane $C_5 H_{12}$

Surface: Nickel, 4/0 polished

System pressure: 1 atm

Properties of fluid:

$T_{sat} = 97^{\circ}$ F

$\rho = 37.8$ lbm/ft.^{3}

$\rho_v = 0.187$ lbm/ft.^{3}

$\sigma = 9.79 \cdot 10^{-4}$ lb/ft.

$L = 146$ btu/lbm $= 1136 \cdot 10^{-3}$ ft. lb/lbm

$\nu = 4.41 \cdot 10^{-6}$ ft.^{2}/sec.

$k = 1.097 \cdot 10^{-6}$ ft.^{2}/sec.

$c = 0.527$ btu/lbm

$\gamma = 8.1 \cdot 10^{-3}$ $1/F^{\circ}$ (From Ref. (17))

Data point 1 = $q_R = 0.390$ btu /(ft.^{2} sec.)

$T_w = 111^{\circ}$ F

$T_{sat} = T_{\infty} = 97^{\circ}$ F

$n = 430$ 1/ft.^{2}

$n_a = 0$

$n_i = 430$ of $R_c = 0.365 \cdot 10^{-5}$ ft. from(17)

$q_P = 0.390$ btu /(ft.^{2} sec.)

Data point 2 = $q_R = 0.865$ btu/(ft.^{2} sec.)

$T_w = 119^\circ$ F

$T_{sat} = T_\infty = 97^\circ$ F

$n = 1580$ 1/ft.^{2}

$n_a = 430$ 1/ft.^{2} of $R_c = 0.365 \cdot 10^{-5}$ ft.

$f = 39.8$ 1/sec.

from (17),(11), (12),(62), (37), and (67)

$n_i = 1150$ 1/ft.^{2} of $R_c = 0.233 \cdot 10^{-5}$ ft.

from (17)

$R_d = 2.60 \cdot 10^{-3}$ ft. from (62)and (37)

$q_P = 0.806$ btu / (ft.^{2} sec.)

Data point 3 = $q_R = 1.208$ btu /(ft.^{2} sec.)

$T_w = 122^\circ$ F

$T_{sat} = T_\infty = 97^\circ$F

$n = 2480$.

$n_a = 1580$. 430 of $R_c = 0.365 \cdot 10^{-5}$ ft., $f = 43.0$ 1/sec.; 1150 of $R_c = 0.233 \cdot 10^{-5}$ ft., $f = 42.6$ 1/sec.

$n_i = 900$ of $R_c = 0.205 \cdot 10^{-5}$ ft.

$R_d = 2.79 \cdot 10^{-3}$ ft.

$q_P = 1.258$ btu /(ft.^{2} sec.)

Data point 4 = $q_R = 1.500$ btu /(ft.^{2} sec.)

$T_w = 124^\circ$ F

$T_{sat} = T_\infty = 97^\circ$F

$n = 3800$.

$n_a = 2480$. 430 of $R_c = 0.365 \cdot 10^{-5}$ ft., $f = 45.4$ 1/sec.; 1150 of $R_c = 0.233 \cdot 10^{-5}$ ft., $f = 45.2$ 1/sec.

$$\left\{\begin{array}{l} \\ \left\{\begin{array}{l} \\ 900 \text{ of } R_c = 0.205 \cdot 10^{-5} \text{ ft.} \\ f = 44.9 \text{ 1/sec.} \end{array}\right. \\ n_i = 1320 \text{ of } R_c = 0.1903 \cdot 10^{-6} \text{ ft.} \end{array}\right.$$

$R_d = 283 \cdot 10^{-3}$ ft.

$q_P = 1611$ btu /(ft.^{2} sec.)

Data point 5 = $q_R = 1.815$ btu /(ft.^{2} sec.)

$T_w = 125.6\ ^\circ F,\ T_{sat} = T_\infty = 97\ ^\circ F$

$n = 5760.$

$$\left\{\begin{array}{l} n_a = 3800 \left\{\begin{array}{l} 430 \text{ of } R_c = 0.365 \cdot 10^{-5} \text{ ft.} \\ f = 47.4 \text{ 1/sec.} \\ 1150 \text{ of } R_c = 0.233 \cdot 10^{-5} \text{ ft.} \\ f = 47.3 \text{ 1/sec.} \\ 900 \text{ of } R_c = 0.205 \cdot 10^{-5} \text{ ft.} \\ f = 47.1 \text{ 1/sec.} \end{array}\right. \\ n_i = 1960 \quad 1320 \text{ of } R_c = 0.1903 \cdot 10^{-5} \text{ ft.} \\ \qquad\qquad f = 46.3 \text{ 1/sec.} \end{array}\right.$$

$R_d = 2.855 \cdot 10^{-3}$ ft.

$q_P = 2.125$ btu /(ft.^{2} sec.)

A bubble initiation diagram of these points is shown in Fig. 27.

A comparison of experimental results with theoretical ones is shown in Fig. 28.

5. Description of Apparatus and Method of Experimentation

a. Experimental Set-Up

The experimental set-up is shown in Fig. 29. The heating surface was made by electroplating a layer of 16 k gold of 0.005 inch thickness on the top surface of a thin flanged cylindrical copper block. The reason for gold plating was to minimize the effects of oxidation so that the surface conditions will remain the same from the beginning to the end of each test. At the bottom of copper block, seven 120 watt chromelux

electrical heaters were imbedded in holes in the copper block. The heat generated by these heaters was transferred to the top surface by pure conduction. The reduction of cross section of copper block underneath the heating surface was for the purpose of intensifying the heat flux at the heating surface. A thin flange surrounds the heater to eliminate undesired bubble nucleation which might occur at a boundary. This flange was very thin so that the temperature near the edge of the heating surface was low enough to prevent bubble initiation. A piece of Teflon heat insulator was inserted between the lower face of this thin flange and pool base. A detailed drawing of the heating surface and the shank part of copper block is shown in Fig. 30.

A thermo-bottle filled with ice was used for the cold junction of the thermocouples which were connected with a potentiometer through a six-way switch. A drain hole valve was also attached to the bottom of the test section. In order to predict the surface temperature, three thermocouples T_1, T_2, and T_3 were inserted in the holes on the shank part of copper block, a three point interpolation formula was used to determine the wall temperature T_w. These thermal couple holes were 1/16 inch in diameter, 19/32 inch in depth and were spaced 1/4 inch apart. All dimensions were measured from the heating surface. The bottoms of these three holes were at the center line of the shank. In the fluid, another thermocouple, T_4, was used to measure the temperature of main body of fluid, T_∞ . It was located one inch above the heating surface. All thermocouples were made of No. 30 Chrome-Alumel wire. In order to avoid excessive corrosion, the thermocouple T_4 was shielded in a 1/16 inch stainless steel tube with Teflon seal at the outer end.

The fluid was contained in a 3 inch diameter and 20 inch length, specially heat-treated, high strength glass tube.

Observations and photographs could be made through a so-called "fluid crystal". This was a glass box filled with the same fluid as that in testing section and so placed as to eliminate distortion due to curvature. The front wall was flat, the rear wall was made of a segment of circular tube with a radius of curvature just equal to the outside radius of the testing tube, such that the distortion of bubble shape due to light refraction of tube was eliminated. With this device, an accurate measurement of bubble dimension could be obtained from high speed photography.

A helically wound copper tube in the upper part of the testing tube was used as a condenser. The saturation temperature of the fluid T_{sat} was controlled by varying the system pressure from 1 atmosphere to 1/4 atmosphere through an asperator vacuum pump. The temperature of the main body of fluid T_{∞} was controlled by varying the flow rate of the cooling water through a cock. The wall temperature T_w was controlled by varying the electrical power of the heaters through a variac.

b. Surface Preparation

Boiling data are difficult to reproduce due to changes in the surface conditions. There are two ways in which these changes appear; namely, changes due to contamination and cavity reactivation. Contamination can be eliminated by proper choice of the metal for the heating surface, reactivation of a nucleate cavity can not be eliminated by the following method.

The 16 k gold plated surface was first finished by 200 grit emery paper which was continuously wetted by a a water jet. The direction of stroke was kept constant. The surface was finished by stroking in one direction till all scratches were eliminated then rotating 90^{o} to eliminate all the scratches in the other direction. The whole piece was then washed in a water jet. Following exactly the same procedure, the surface was finished by

400 grit and 600 grit emery paper. The surface was then cleaned by hot water jet, alcohol jet and hot air jet and was then put on the No. 4 diamond compound wheel. The diamond compound should be put on the center area of grinding wheel and diluted by kerosene before starting grinding operation. The piece was held gently near the edge area of wheel, kerosene was injected on the wheel clothe occasionally. Operation was continued until the scratches due to 600 grit emery paper disappeared completely. Then the piece was taken off from No. 4 diamond compound wheel, the hot water jet, the alcohol jet and the hot air jet were then each put on the surface. After the washing process, the piece was then put on the No. 6 diamond compound wheel and then No. 8 wheel using the same sequence of operations as on the No. 4 wheel.

An unclean piece will leave some dust particles on the wheel which sometimes make some unremovable scratches on the surface. To make a good surface, one needs usually more than 10 hours. Patience and cleanliness are the two most important characteristics of a surface worker. Scratches due to the grinding compound can be removed only by its next number grinding compound as recommended here. No. 4 diamond compound scratches can not be removed by No. 8 diamond compound wheel in a reasonable length of time without introducing No. 6 diamond compound wheel.

At the last few minutes of grinding process on the No. 8 diamond compound wheel, the kerosene jet was applied all over the center area of the wheel, such that the diamond compound was washed to a very dilute condition, the piece was then put near the center part of the wheel where the rubbing speed is lower, then a heavier pressure was applied. After one to two minutes, the

surface would become shining, mirror-like smooth. It was washed by hot water jet, alcohol jet and hot air jet, it was then introduced in the pool of a ultrasonic cleaner for 2 minutes. This process would help to wash out small diamond dust particles and bits of metal which were trapped in the cavities on the surface. Then the surface was washed again by alcohol and Methyl ether jet. The surface at this stage was assumed to be the surface required.

After each test, the surface was renewed by going through all the steps immediately after No. 6 diamond compound wheel. It needed only 20 minutes to finish the job.

In order to keep surface condition unchanged, every element which is in the boiling system should be cleaned by washing soap, hot water jet and distilled water jet before each test.

c. Method of Experimentation

After making a new surface and washing all the parts, they were assembled, distilled water was introduced into the top of the test section. Two hours of vigorous boiling with a moderate heat flux was maintained for degassing purposes, then the heat flux was reduced until there were no active cavities on the surface, then the heat flux was increased gradually until the first active cavity appeared on the surface. This was the starting point of each test. A steady state condition was assumed to be reached two hours after the heat flux was changed.

During each run the following measurements were made. Power, fluid temperature, heater-unit temperatures, system pressure, number of active centers, and number of new sites arising from the change in heat flux. Technically the later are called the initiated cavities which generate bubbles with very low frequencies such

that the contribution to the heat transfer is negligible . The heat transfer to the fluid through the heating surface was determined by the simple conduction formula knowing the temperature gradient in the shank of copper block. The wall temperature T_w within a circular area of 7 3/16" diameter on the center part of the heating surface was assumed to be uniform .

d. Photographic Technique

High speed photographs were taken with a Wollensack camera. A Kodak Tri-X negative 100' film for high speed photography was used. About 2400 frames per second was taken which necessitated a reduction of voltage supplied to the Wollensack camera motor to about 70 volts through a variac. A 500 watt illuminating lamp was installed at the rear of the test section at about 6 inches away from the tube center, so that the heating surface looked shining bright. The focus of the camera was very carefully adjusted such that no relative motion between the circle on the focusing lens and the bubble to be photographed was observed. Each two marks of time on the film represent 1/60 sec.

The camera was placed as close as possible to the test section without losing the sharp focus required. A reference wire of 0.040 inch in diameter was placed besides the bubble which was to be photographed. The bubble diameter measurements were made by projection on a microfilm projector. A geometric mean value of bubble diameters in three principal axis directions was considered as the bubble diameter for volume calculation.

e. Temperature Calibration, Wall Temperature Prediction and Heat Flux Determination

i, Temperature Calibration

For this special kind of chrome-alumel thermocouple, the following data were recorded.

Reading at boiling point of water = 5.209 milli-volts

Reading at melting point of tin = 12.410 milli-volts

Reading at freezing point of water = 0.000 milli-volts

Atmospheric pressure P = 77.66 cm. Hg

Boiling point of water at P = 77.66 cm. Hg

is from $T = 100.000 + 0.03686 (P - 76.00) - 0.0000220 (P - 76.00)^2 = 100.061^{\circ}C$

Melting point of tin at atmospheric pressure = $231.89^{\circ}C$

Freezing point of water at atmospheric pressure = $0.000^{\circ}C$

From Reference (14), a three point interpolation formula gives

$$T = 0.07267 V (299.540 - V) \quad ^{\circ}C \qquad (89)$$

Where V is the reading of thermocouple from potentiometer (m.v.)

T is the corresponding temperature C° .

ii, Wall Temperature Prediction

Referring to the sketch of heat surface and heat conductor shank which is shown in Fig. 30, the following dimensions were obtained by an accurate measurement.

$S_1 = 0.242''$

$S_2 = 0.234''$

$S_3 = 0.230''$

The location of each thermocouple and the heating surface can be described by coordinate X's, say

$x_1 = 0$, $x_2 = S_1 = 0.242''$,

$x_3 = S_1 + S_2 = 0.476''$, $x_w = S_1 + S_2 + S_3 = 0.706''$

If the corresponding temperature sat X_1, X_2, X_3, and X_w are T_1, T_2, T_3, and T_w, then with help of Ref. (14), the wall temperature can be extrapolated by Lagrangian method as

$$T_W = T_1 \frac{(X_W - X_2)(X_W - X_3)}{(X_1 - X_2)(X_1 - X_3)} + T_2 \frac{(X_W - X_1)(X_W - X_3)}{(X_2 - X_1)(X_2 - X_3)} + T_3 \frac{(X_W - X_1)(X_W - X_2)}{(X_3 - X_1)(X_3 - X_2)}$$

substituting the value of X_1, X_2, X_3, and X_w into above equation yields

$$T_W = 0.9265\,T_1 - 2.8675\,T_2 + 2.9410\,T_3 \qquad (90)$$

iii, Heat Flux Determination

From conduction equation, one has

$$Q = A_s K_c \frac{\Delta T}{\Delta X} = A_s K_c \frac{T_1 - T_3}{X_3}$$

A_s = cross section area of shank of conductor = 0.00769 12 ft.^{2}

K_c = conductivity of copper = 219 btu/(^{o}F hr.ft.) = 0.060833 btu/(ft.$\cdot$ ^{o}F$\cdot$sec.)

X_3 = 0.476" = 0.03967 ft.

$T_1 - T_3$ in degree Fahrenheit

$$Q = 0.0118\ (T_1 - T_3)\ \text{btu/sec.} \qquad (91)$$

6. Discussion and Conclusion

a. Discussion

In the preceding sections it has been shown possible to consider the individual processes of bubble initiation, growth, and departure and with nothing other than geometric idealizations and fluid and surface properties, compute a heat flux versus wall temperature curve. The computed and measured heat flux curves compare satisfactorily. In making this comparison however, an extraordinary amount of information was needed. In practical terms, quantities like surface nucleation, properties and bulk temperatures are just not known with sufficient precision to make a boiling curve prediction possible. In addition, only the isolated bubble portion of the pool boiling curve has been studied. If the forced convection or the close packed regions are of interest, then other geometrical ideali-

zations of the fluid mechanics are needed. This all raises the question of where do we go from here ?

The close correlation between theory and experiment and the fact that no arbitrary constants have been used show that no important physics has been forgotten. What further should be done in nucleate boiling ? First, the physics.

i, Bubble Initiation

More experience is needed in the experimental control of surface conditions. Contact angle, drift and surface nucleation properties need more study in order that meaningful experiments can be desired.

ii, Bubble Growth

This appears to be well understood

iii, Bubble Departure

The zero gravity departure prediction should be tested. Forced convection bubble departure should be studied as only a few odd measurements now exist.

Engineering work - better heat flux temperature difference correlations are now possible based on our cleaner understanding of the basis processes. Work with industrial rather than laboratory type data is probably most desirable.

b. Conclusions

i, The nucleate pool boiling curve in the isolated bubble region can be predicted from a knowledge of fluid properties and surface conditions. Resort need not be made to any physically unmotivated quantities.

ii, Dynamic effects on bubble departure size manifest themselves primarily through contact angle variations with the usual Fritz formula still holding.

iii, A formula including dynamic effects in the liquid has been developed that would predict bubble departure at zero gravity for certain fluid properties and temperature distributions.

iv, The waiting period between bubbles is shown to be a known function of cavity size and liquid and surface temperature.

v, Using measured delay times, bubble growth rate can be predicted with good precision.

vi, Using measured contact angles bubble departure size can be predicted.

vii, Contact angle has been found to be a function of velocity across the surface. This in turn has been correlated with viscous effects in terms of a ratio of Webber to Reynolds numbers.

BUBBLE GROWTH TABLE 1

The Experimental Data for Bubble Number 1

t_w = 0.0245 sec.

t_d = 0.0166 sec.

R_d = $3.974 \cdot 10^{-3}$ ft.

Camera speed = 1140 frames/sec.

No. of Frame	t Millisec	Bubble Diameter on Microfilm Projector (m.m) Scale = 8.87 : 1	R Millift
1	0	2.32	0.429
2	0.877	9.48	1.754
3	1.654	13.72	2.538
4	2.631	16.04	2.967
5	3.508	17.80	3.293
6	4.385	18.40	3.404
7	5.262	18.95	3.506
8	6.139	19.57	3.620
9	7.016	19.86	3.674
10	7.893	20.00	3.700
11	8.770	20.36	3.767
12	9.647	20.72	3.833
13	10.524	21.10	3.904
14	11.401	21.65	4.005
15	12.278	21.90	4.052
16	13.155	21.90	4.052
17	14.032	21.80	4.033
18	14.909	21.69	4.013
19	15.786	21.48	$3.974(R_d)$

BUBBLE GROWTH TABLE 2

The Experimental Data for Bubble Number 2

t_w = 0.0437 sec.

t_d = 0.0167 sec.

$R_d = 5.328 \cdot 10^{-3}$ ft.

Camera speed = 1260 frames/sec.

No. of Frame	t Millisec	Bubble Diameter on Microfilm Projector (m.m) Scale = 8.87 : 1	R Millift.
1	0.793	9.26	1.713
2	1.586	14.22	2.631
3	2.379	17.53	3.243
4	3.172	19.76	3.656
5	3.965	21.65	4.005
6	4.758	22.80	4.218
7	5.551	23.87	4.416
8	6.344	24.67	4.564
9	7.137	25.20	4.662
10	7.930	25.48	4.714
11	8.723	25.50	4.718
12	9.516	25.80	4.773
13	10.309	26.10	4.829
14	11.102	26.74	4.947
15	11.895	27.26	5.043
16	12.688	27.40	5.069
17	13.481	27.70	5.125
18	14.274	27.90	5.162
19	15.067	28.53	5.278
20	15.860	28.87	5.341
21	16.653	28.80	$5.328(R_d)$

BUBBLE GROWTH TABLE 3

The Experimental Data for Bubble Number 3

t_w = 0.0275 sec.

t_d = 0.0145 sec.

$R_d = 0.395 \cdot 10^{-3}$ ft.

Camera speed = 1380 frames/sec.

No. of Frame	t Millisec	Bubble Diameter on Microfilm Projector (m.m) Scale = 8.87 : 1	R Millift.
1	0.725	9.52	1.711
2	1.450	14.10	2.609
3	2.175	16.88	3.123
4	2.900	18.45	3.413
5	3.625	19.55	3.617
6	4.350	20.60	3.811
7	5.075	21.73	4.020
8	5.800	22.08	4.085
9	6.525	22.53	4.168
10	7.250	22.75	4.209
11	7.975	23.68	4.381
12	8.700	24.00	4.440
13	9.425	24.10	4.459
14	10.150	24.33	4.501
15	10.875	24.15	4.468
16	11.600	24.74	4.577
17	12.325	25.52	4.721
18	13.050	25.80	4.773
19	13.775	25.88	4.788
20	14.500	25.90	4.792(R_d)

TABLE 4

HISTORY OF BUBBLE GENERATIONS

$T_w = 229.98^{\circ}F$, $T_{sat} = 212^{\circ}F$, $T_{\infty} = 205.02^{\circ}F$

Distilled water on gold surface ground by No. 8 diamond compound

Bubble No.	Camera Speed (frames/sec.)	t_w (sec.)	t_d (sec.)	R_d (Millift.)
1	1140	0.0254	0.0167	3.974
2	1260	0.0436	0.0167	5.328
3	1380	0.0275	0.0145	4.792
4	1500	0.0466	0.0167	3.534
5	1650	0.0735	0.0261	3.691
6	1800	0.0594	0.0172	4.224
7	1920	0.0490	0.0151	4.188
8	2040	0.0633	0.0162	4.658
9	2130	0.0319	0.0155	3.931
10	2190	0.0337	0.0160	5.125
11	2280	0.0672	0.0149	3.321
12	2370	0.0785	0.0167	3.448
13	2520	0.1640	0.0143	3.633
14	2700	0.1250	0.0512 (Three in Tandem)	4.201
15	2770	0.0436	0.0143	3.566
16	2850	0.0393	0.0161	4.782
17	2910	0.0216	0.0158	5.367
18	2910	0.0450	0.0139	3.374
19	2940	0.0756	0.0296 (Two in Tandem)	3.571
20	2940	0.0252	0.0163	4.967
21	2940	0.0354	0.0139	3.883
22	2940	0.0490	0.0129	4.183

Observation from above table shows that the waiting period t_w changes from $17(t_w)_{min.}$ to $130(t_w)_{min.}$

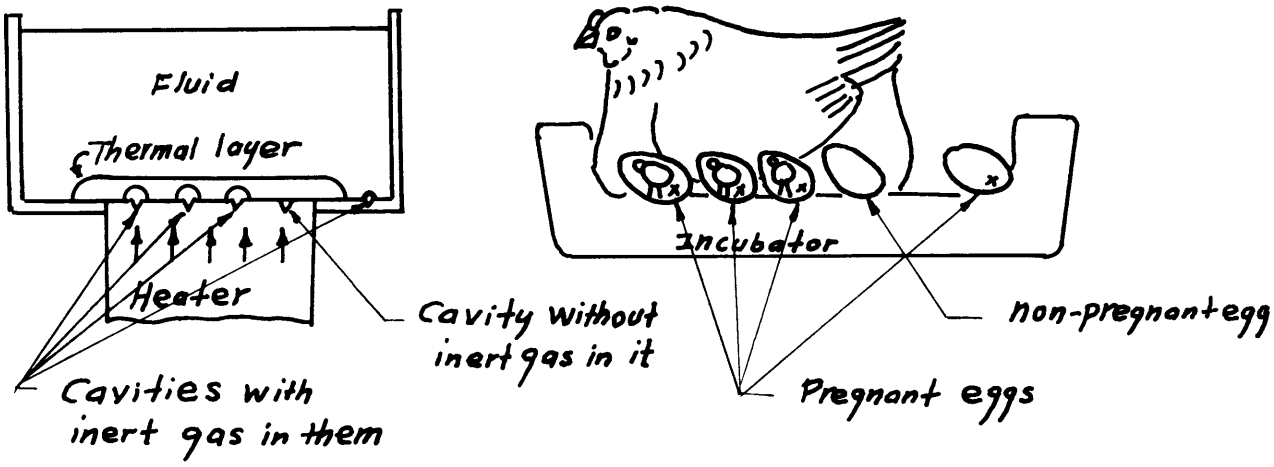

Fig. 1 Analogues Between Bubble Initiation & Egg Incubation

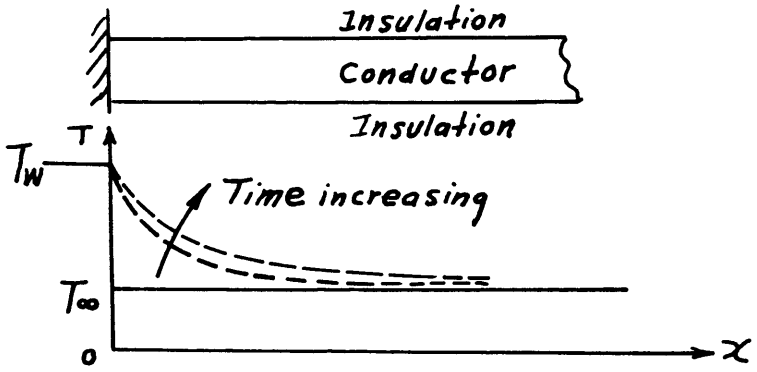

Fig. 2 Temperature Distribution in a Semi-Infinite Conductor

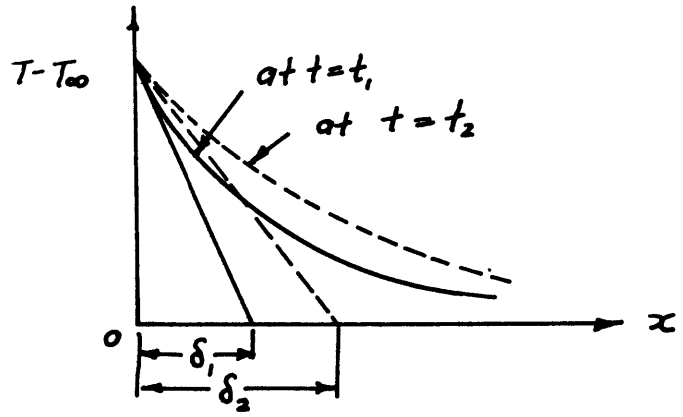

Fig. 3 Transient Thermal Layer

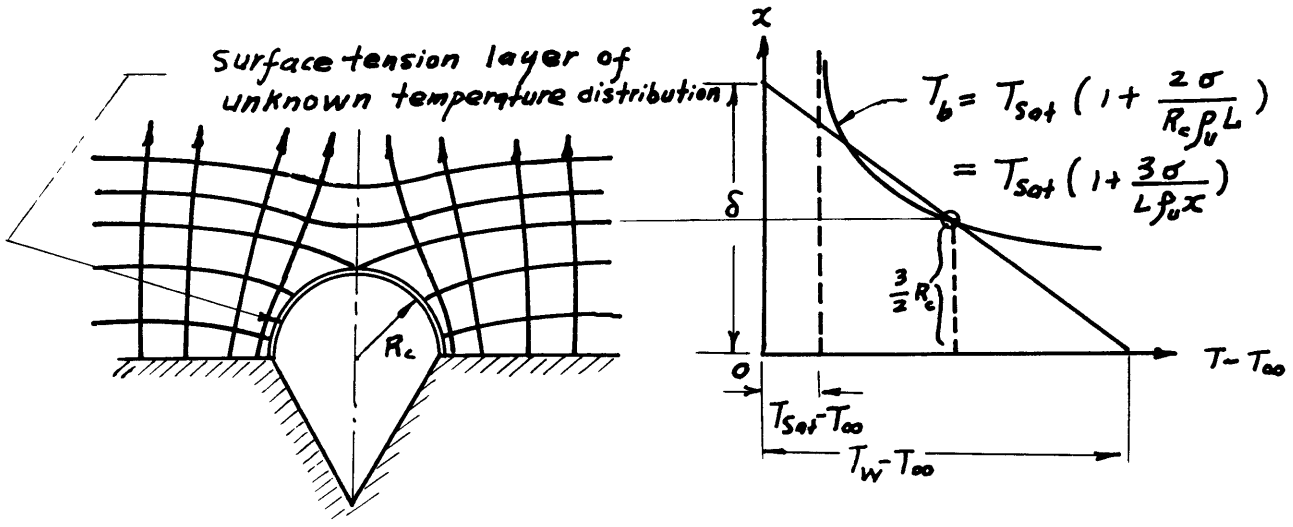

Fig. 4 Temperatures of Fluid and Bubble Near a Heating Surface

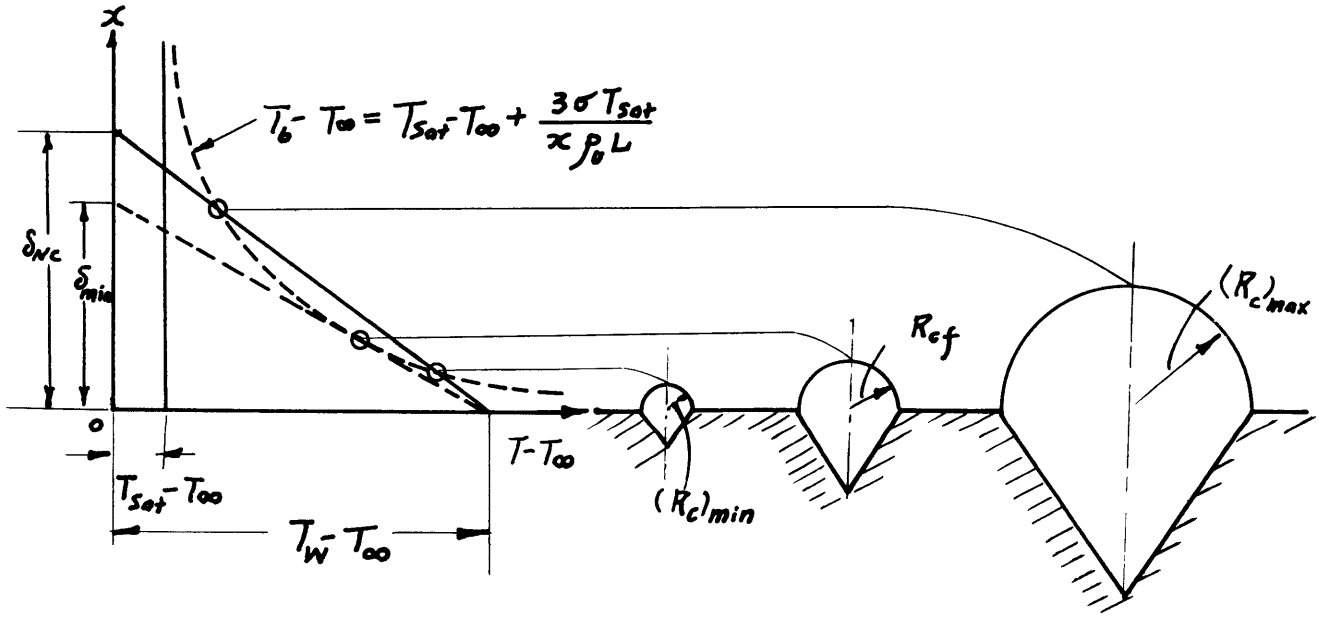

Fig. 5 Initiation of Bubble Growth From Different Cavities

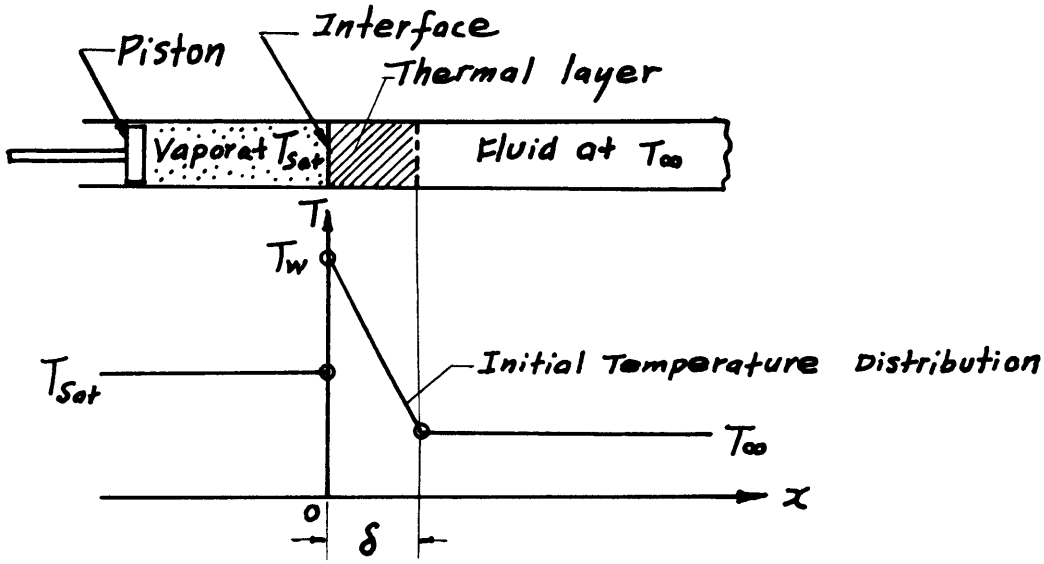

Fig. 6 Simplified Physical Model of Heat Transfer

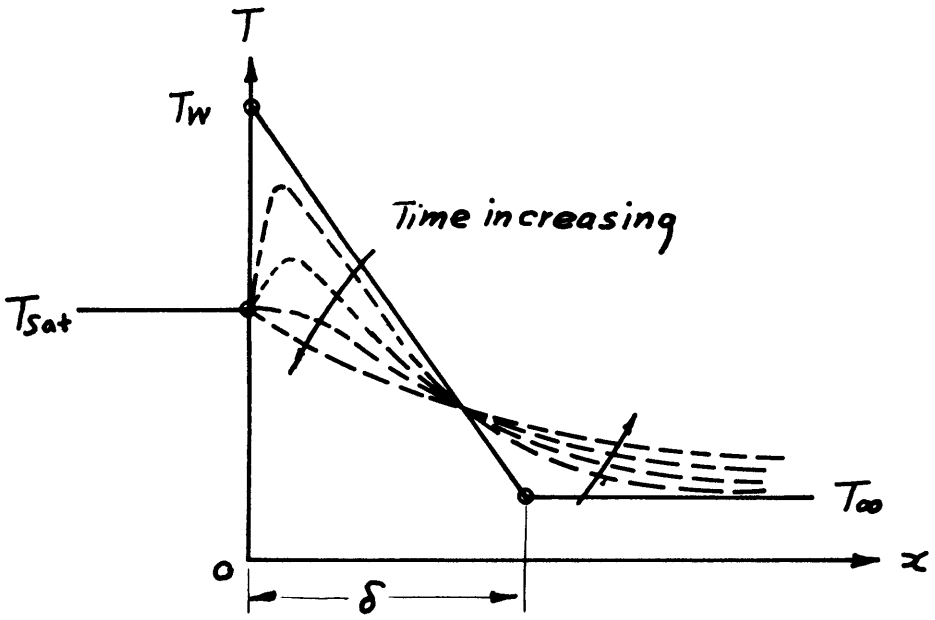

Fig. 7 Temperature Distribution in the Fluid Surrounding a Bubble

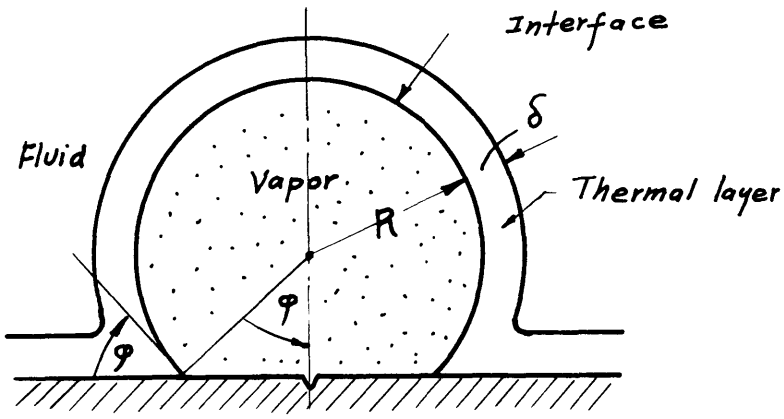

Fig. 8 Simplified Model of a Bubble Growth

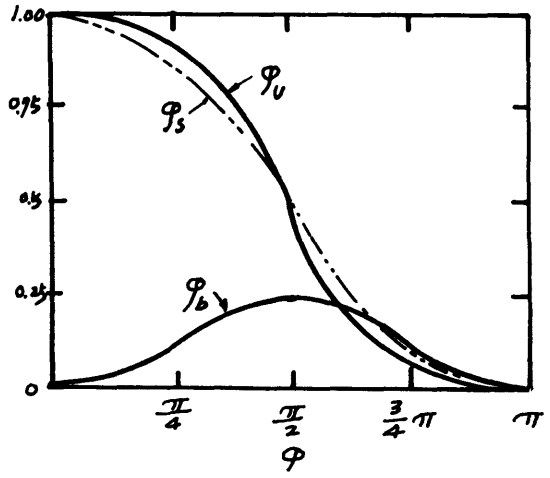

Fig. 9 Configuration Factors of Spheric Bubble

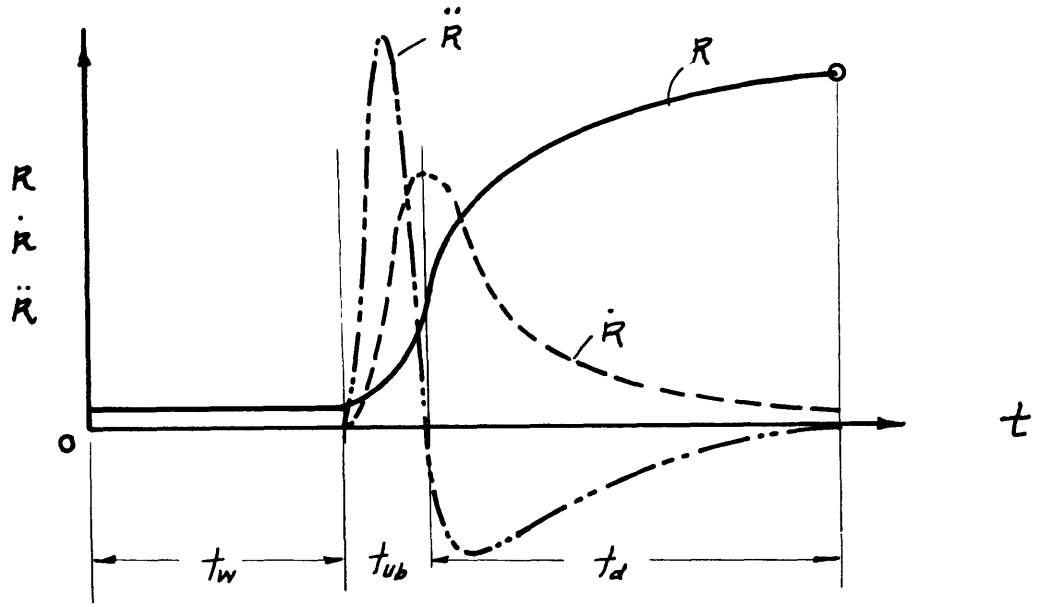

Fig. 15 Bubble Growth Curve When the Dynamic Effect and Surface Tension are Considered

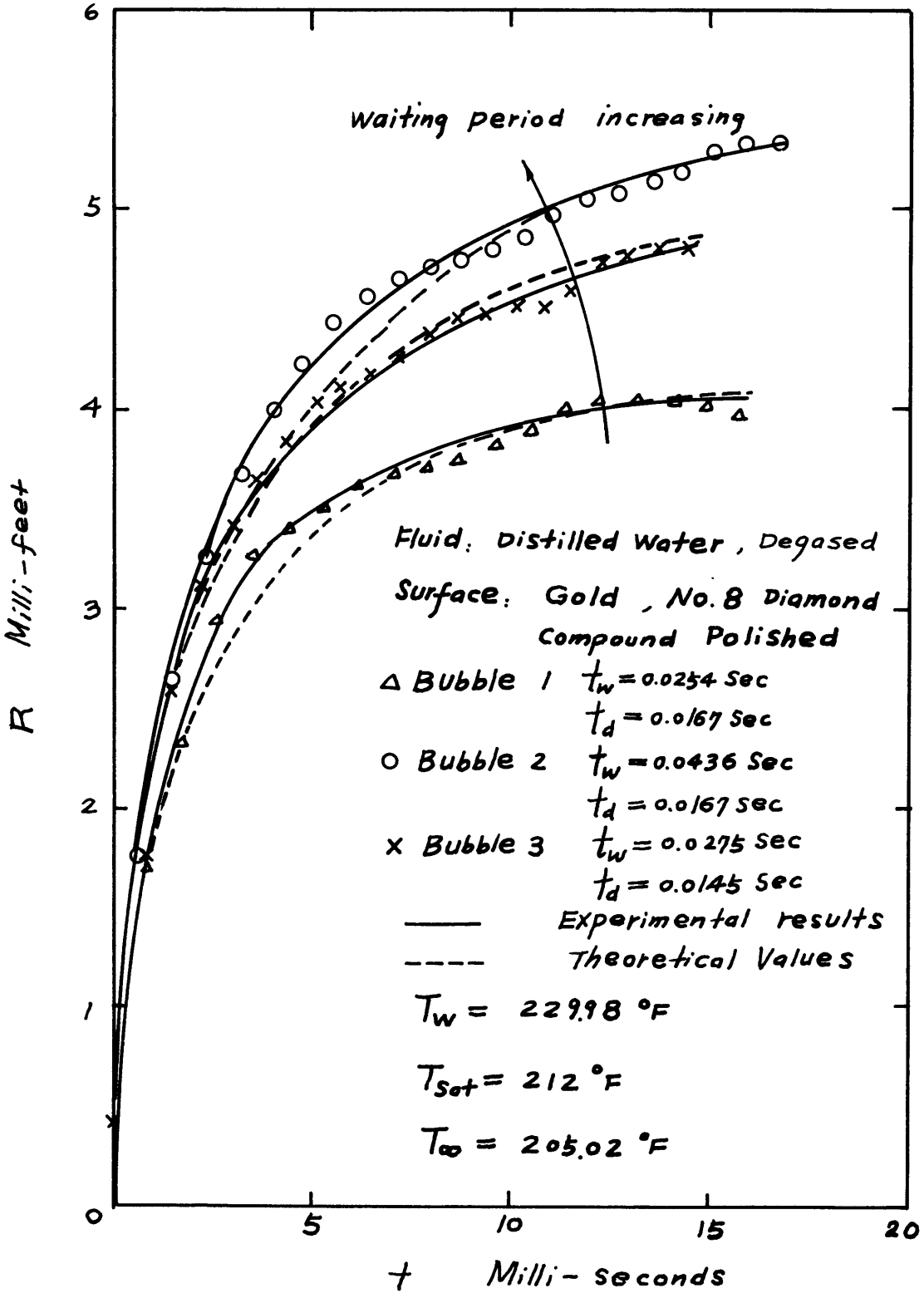

Fig. 11 Bubble Growth Plot

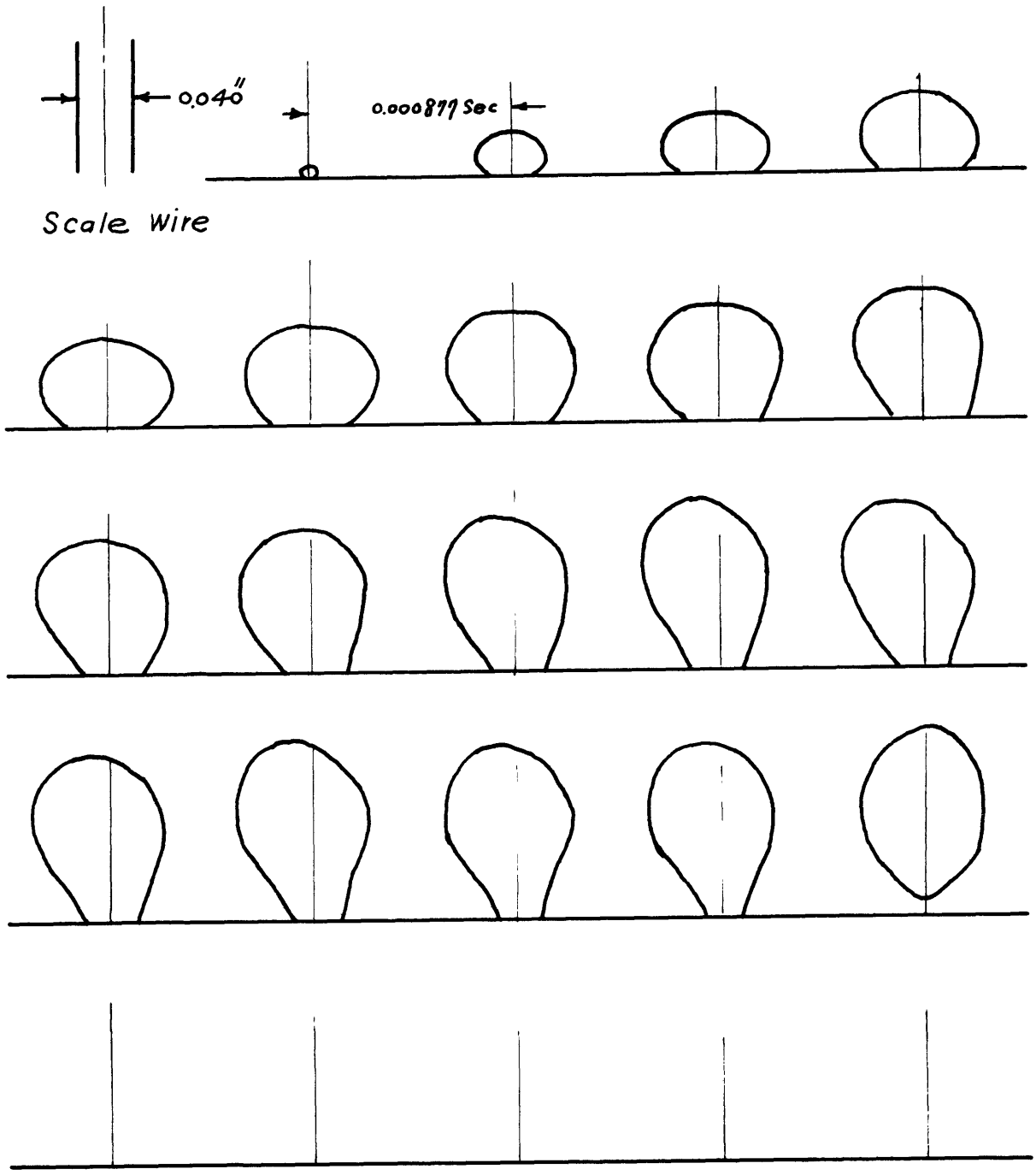

Bubble Number 1:

Camera Speed = 1140 frames/sec

Waiting Period = 29 frames = 0.0254 Sec

Departure Period = 19 frames = 0.0166 Sec

Departure Radius = $3.99 \cdot 10^{-3}$ ft

Fig. 12 History of Growth of Bubble Number 3

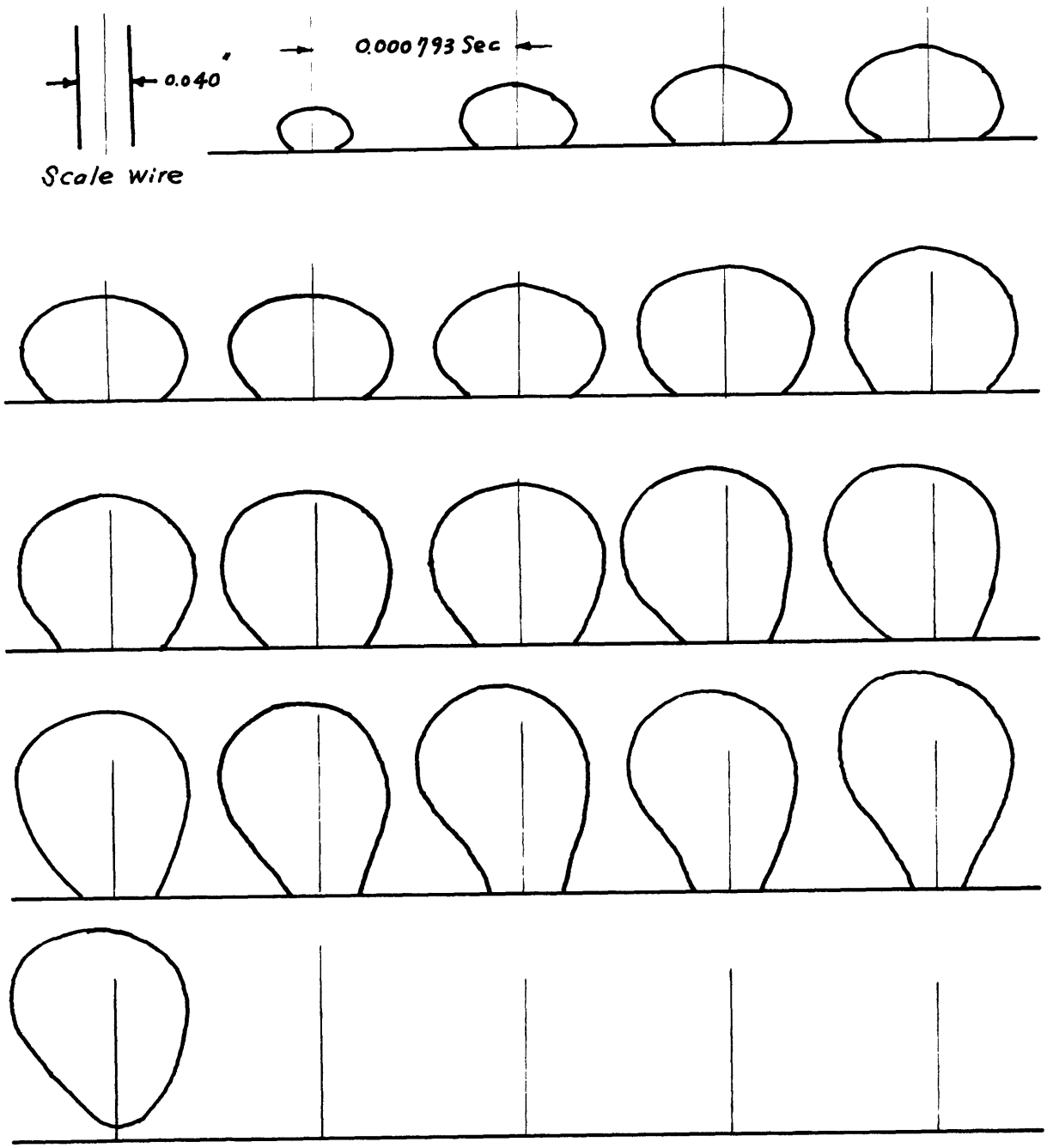

Bubble Number 2,

Camera Speed = 1260 Frames/Sec

Waiting Period = 55 Frames = 0.0437 Sec

Departure Period = 21 Frames = 0.0167 Sec

Departure Radius = $5.33 \cdot 10^{-3}$ ft

Fig. 13 History of Growth of Bubble Number 2

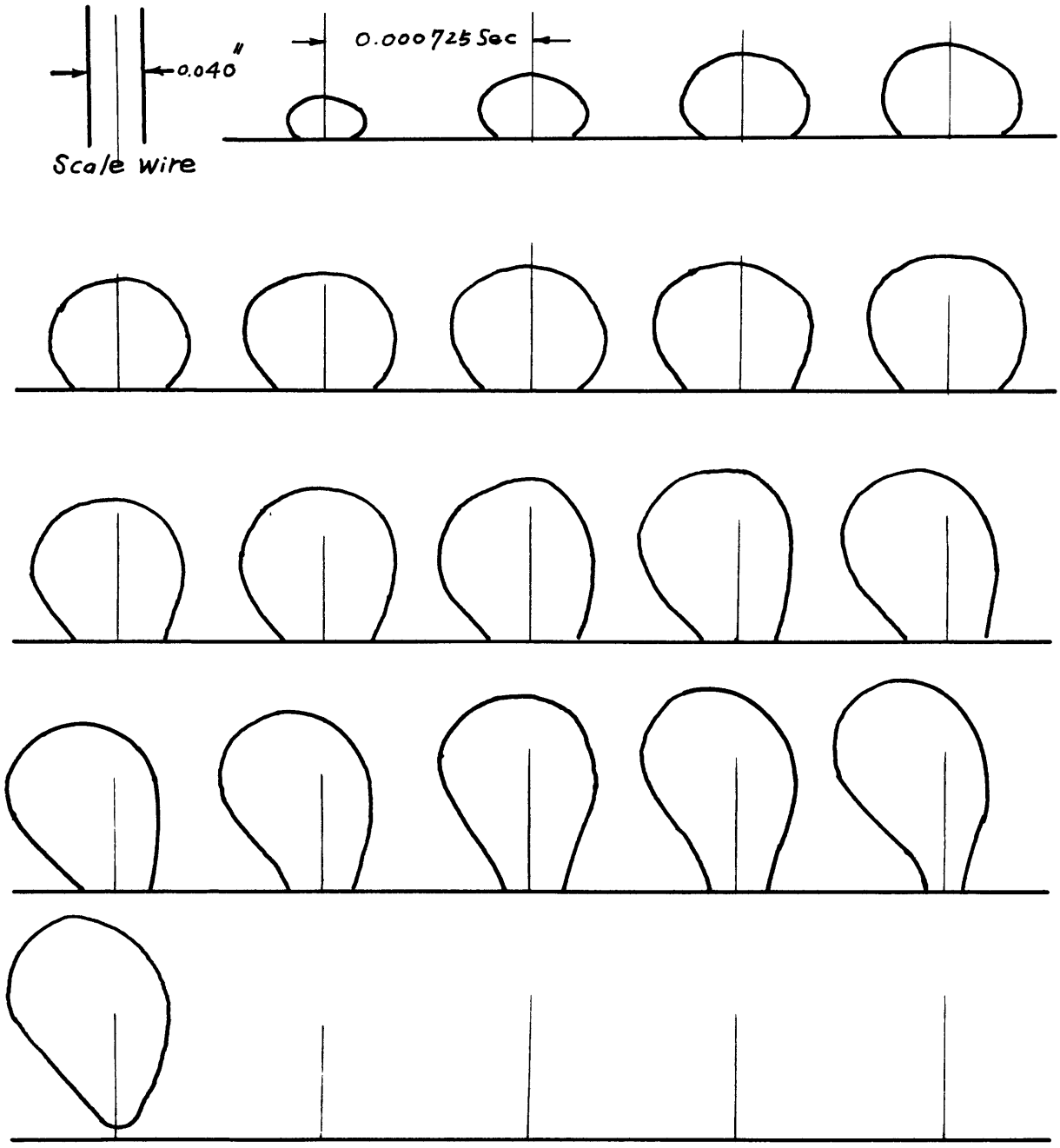

Bubble Number 3:

Camera Speed = 1380 Frames/Sec
Waiting Period = 38 Frames = 0.0275 Sec
Departure Period = 20 Frames = 0.0145 Sec
Departure Radius = $4.79 \cdot 10^{-3}$ Ft

Fig.14 History of Growth of Bubble Number 1

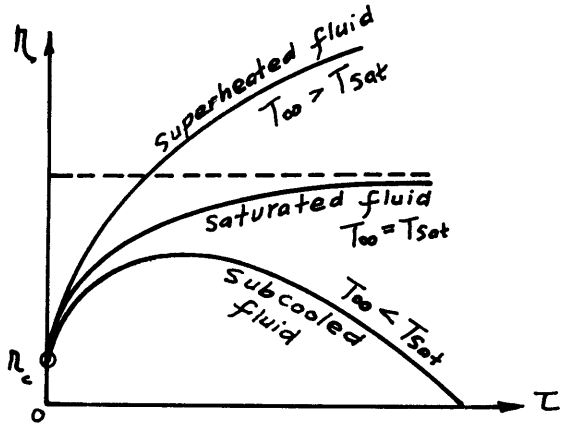

Fig. 10 Normalized Bubble Growth Curves

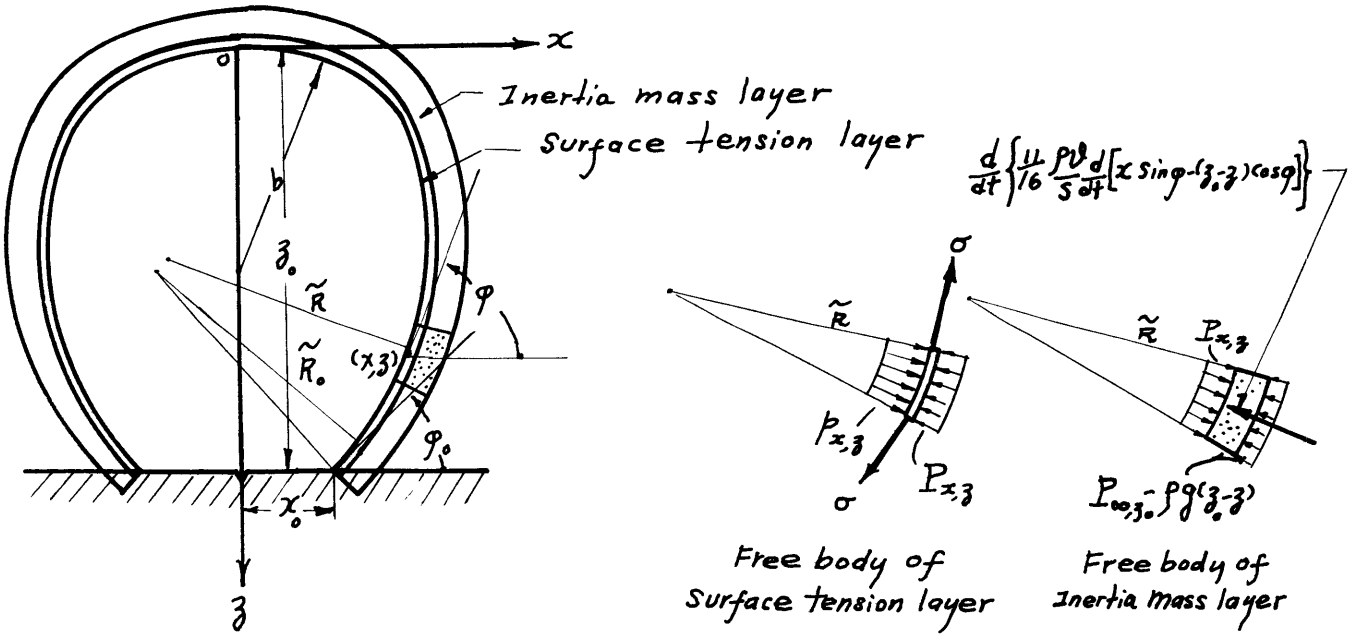

Fig. 16 Dynamic Load on a Growing Bubble

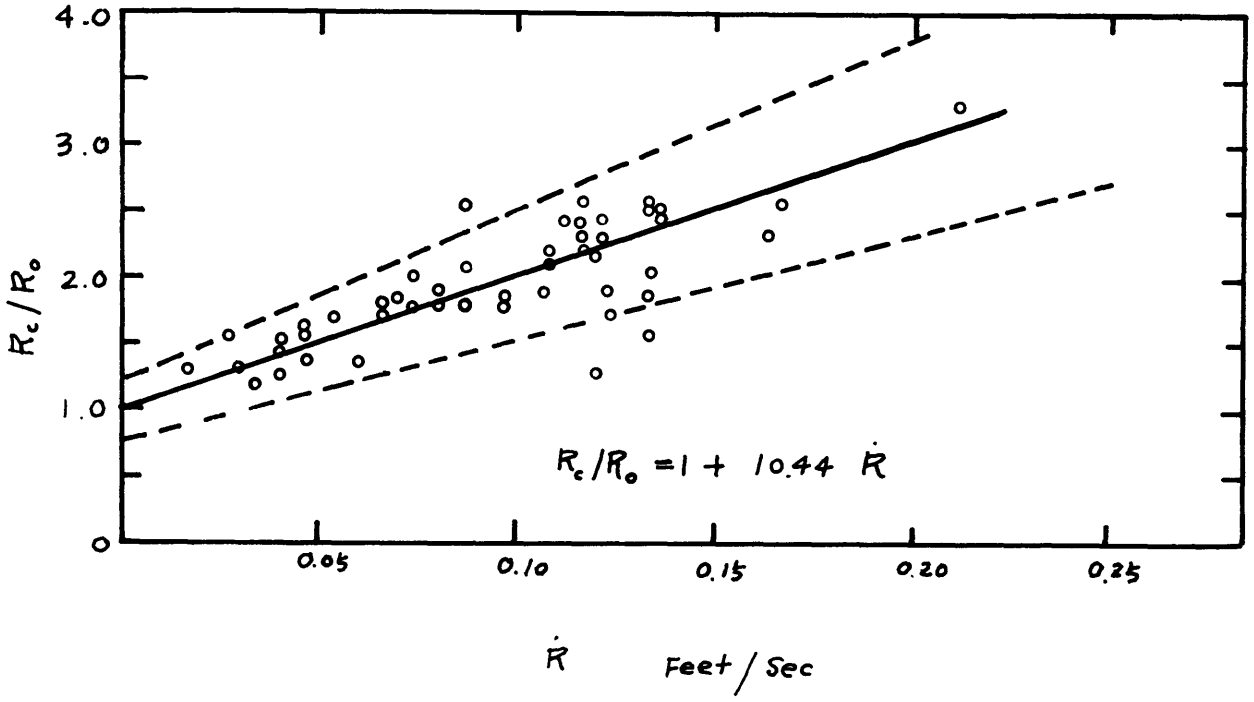

Fig. 17 Staniszewski's Departure Criterion

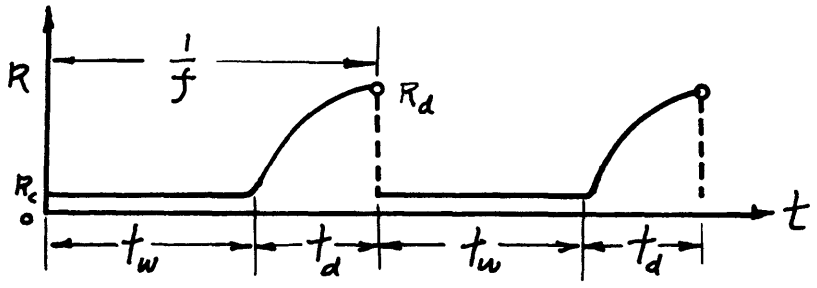

Fig. 18 Bubble Generating Cycles

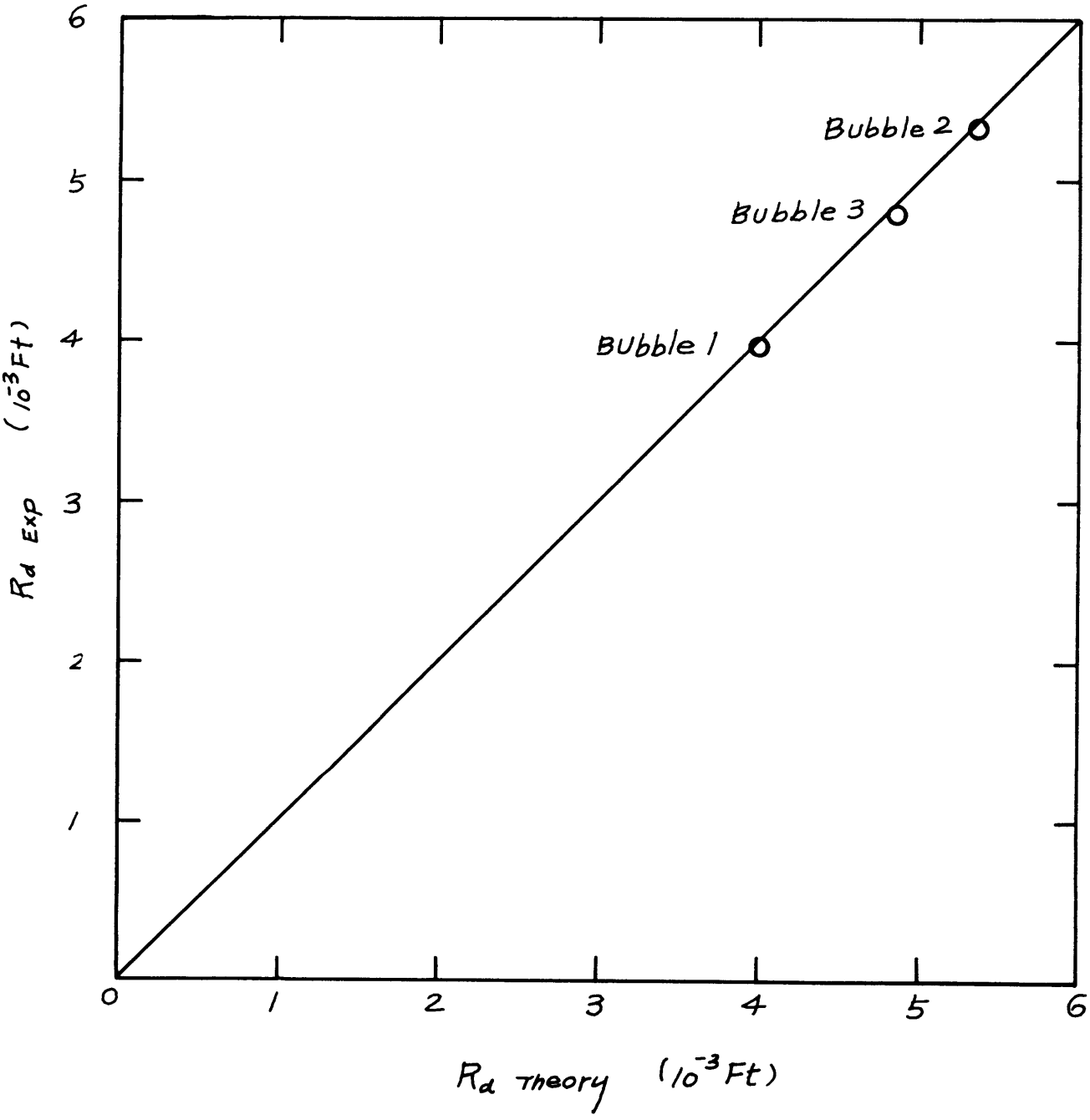

Fig.19 Verification of Bubble Departure Theory

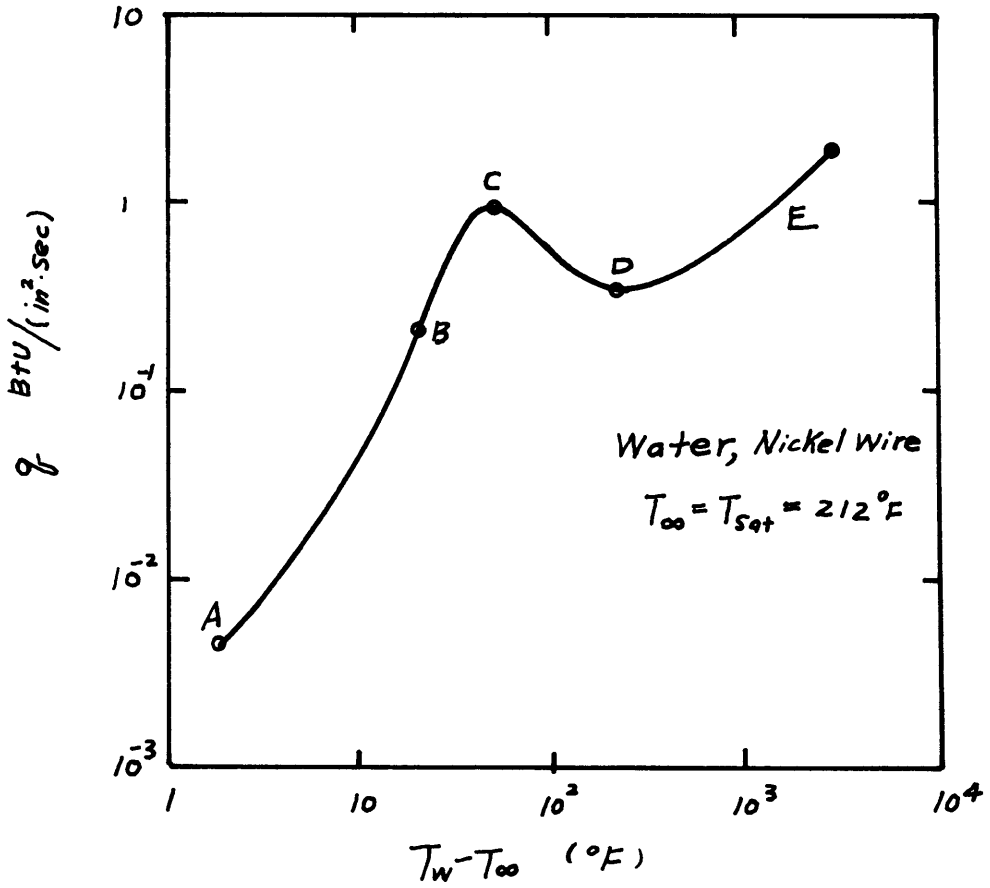

Fig. 20 Boiling Curve

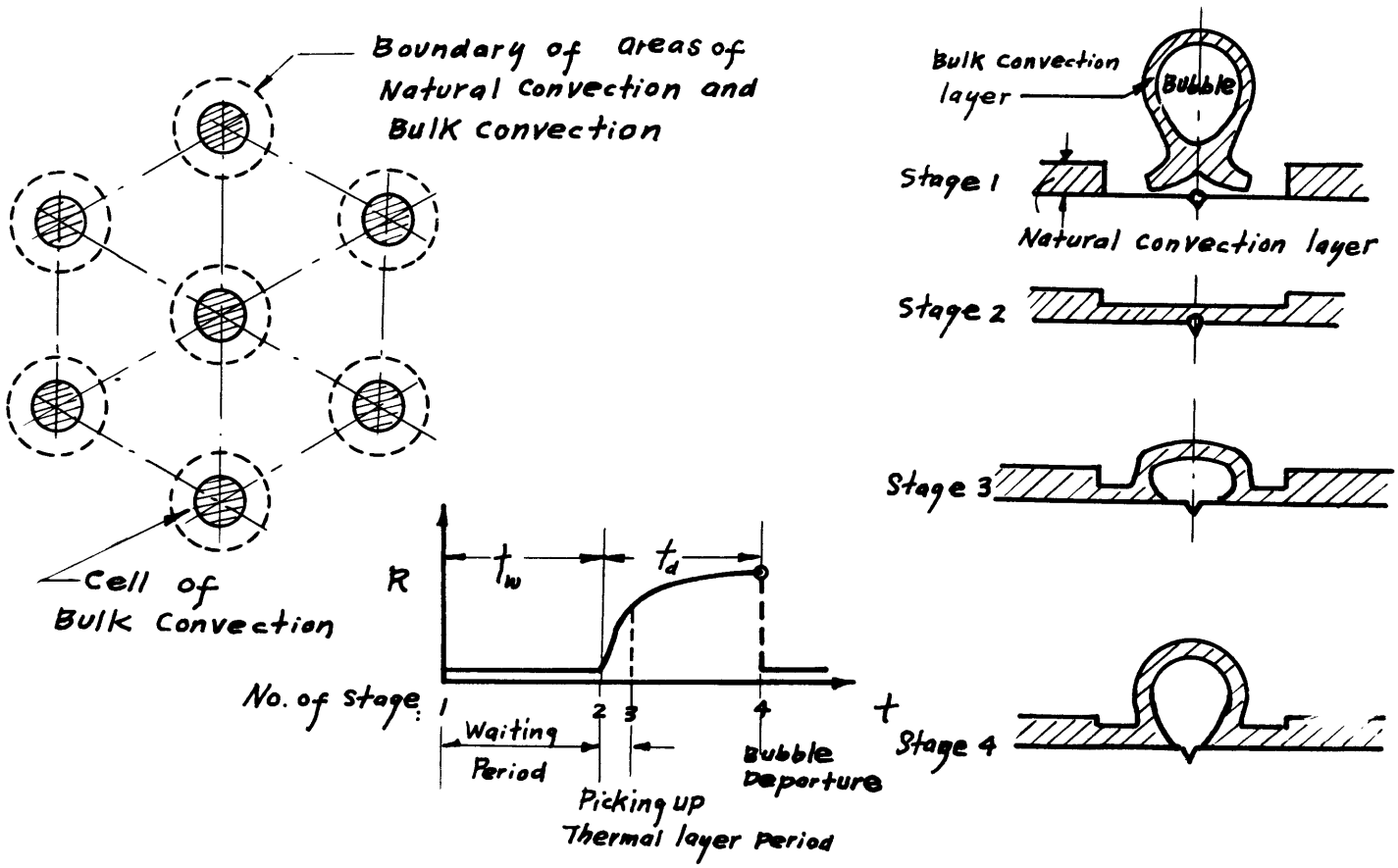

Fig. 21 Physical Model of Bulk Convection Mechanism

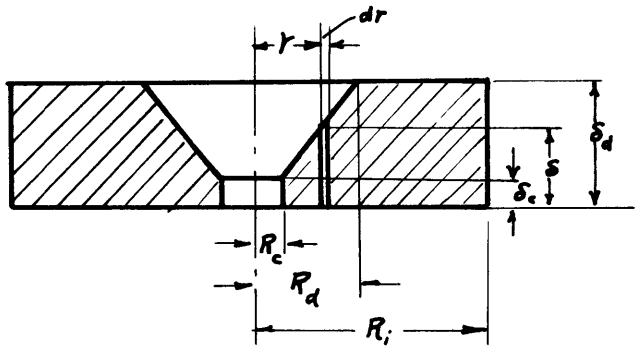

Fig. 22 Transient Thermal Layer of a Bulk Convection Cell

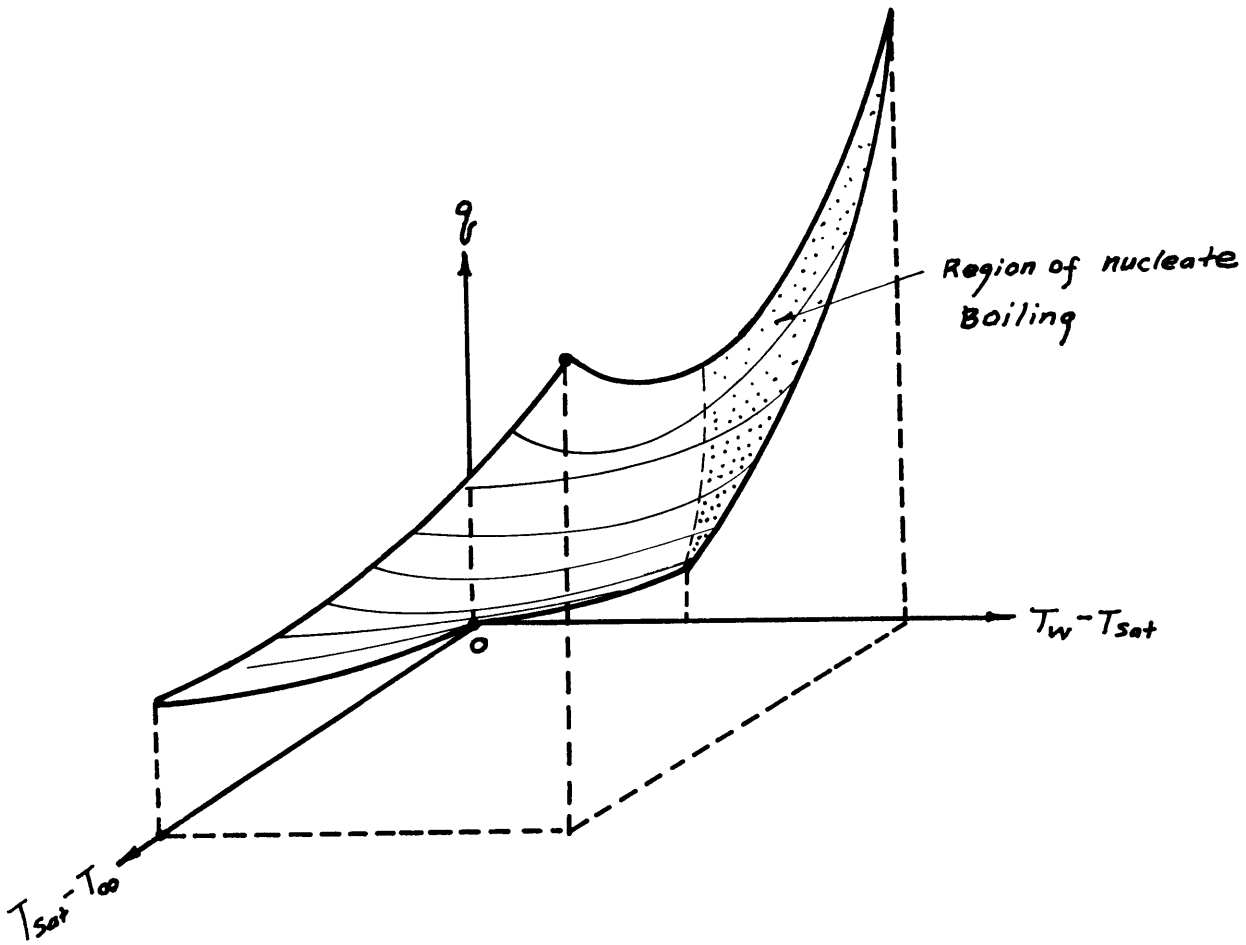

Fig. 23 Effects of Wall Superheat & Mainfluid Subcooling on Heat Transfer

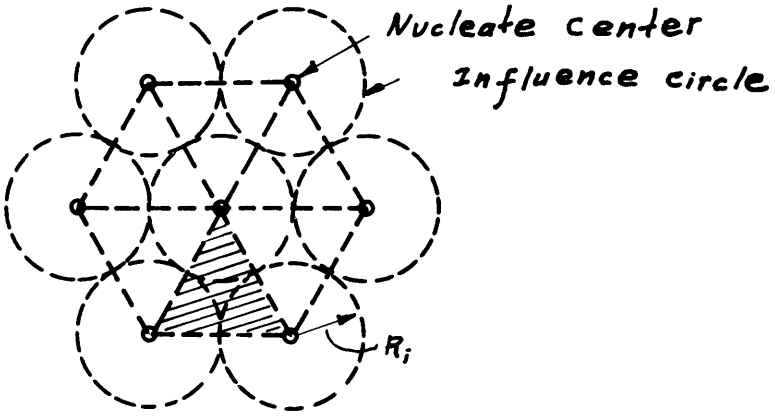

Fig. 24 Nucleate Cells at Close Packed Condition

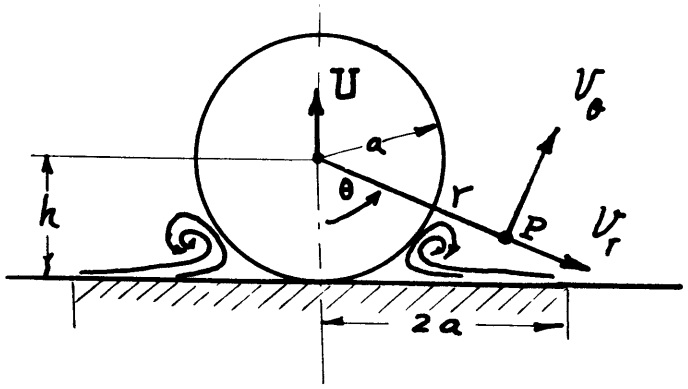

Fig. 25 Scavenging Effect of a Departing Bubble

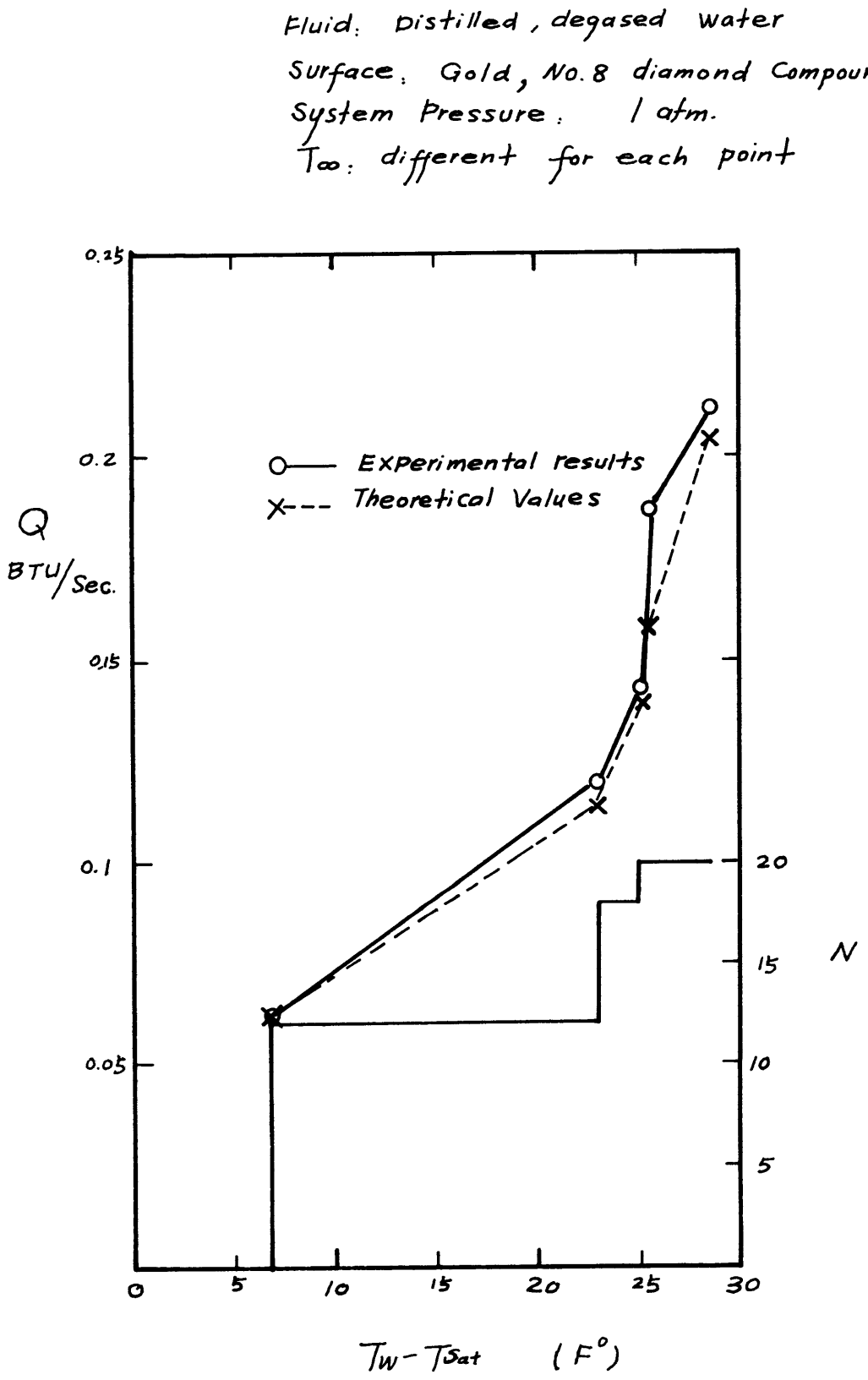

Fig. 26 Verification of Bulk Convection Theory by Han's Data

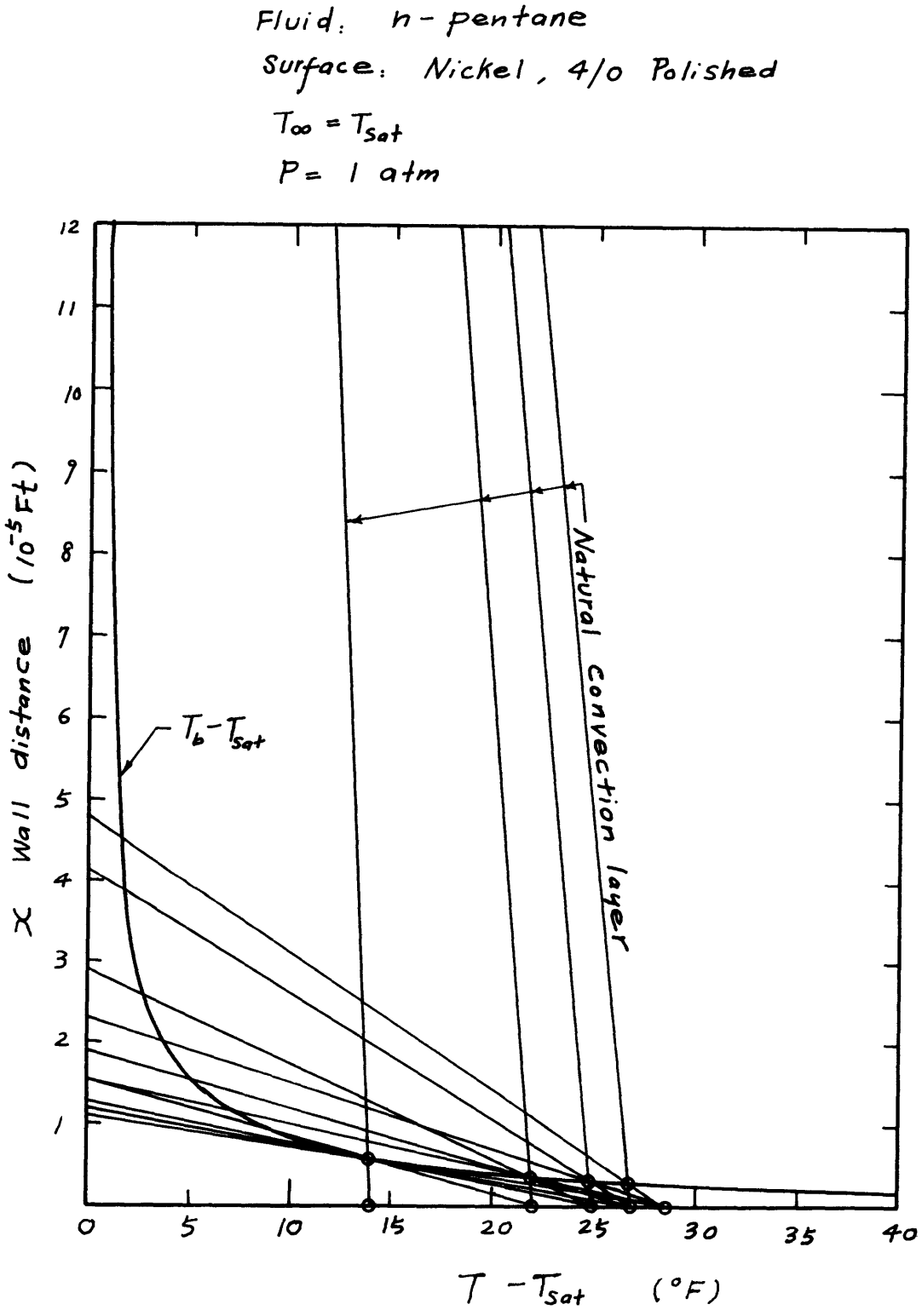

Fig. 27 Bubble Initiation Diagram of Corty and Foust's Data

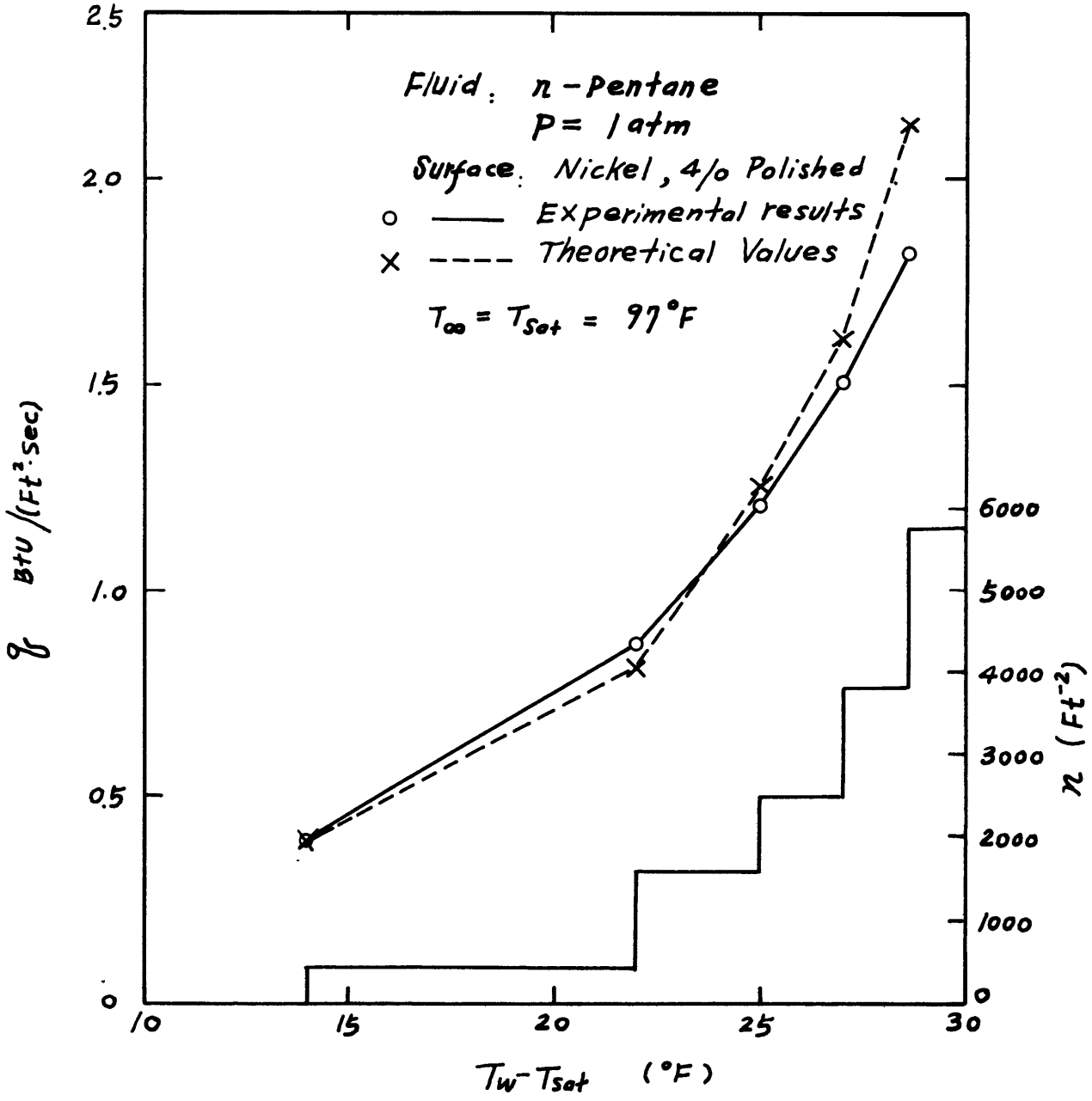

Fig. 28 Verification of Bulk Convection Theory by Corty and Foust's Data

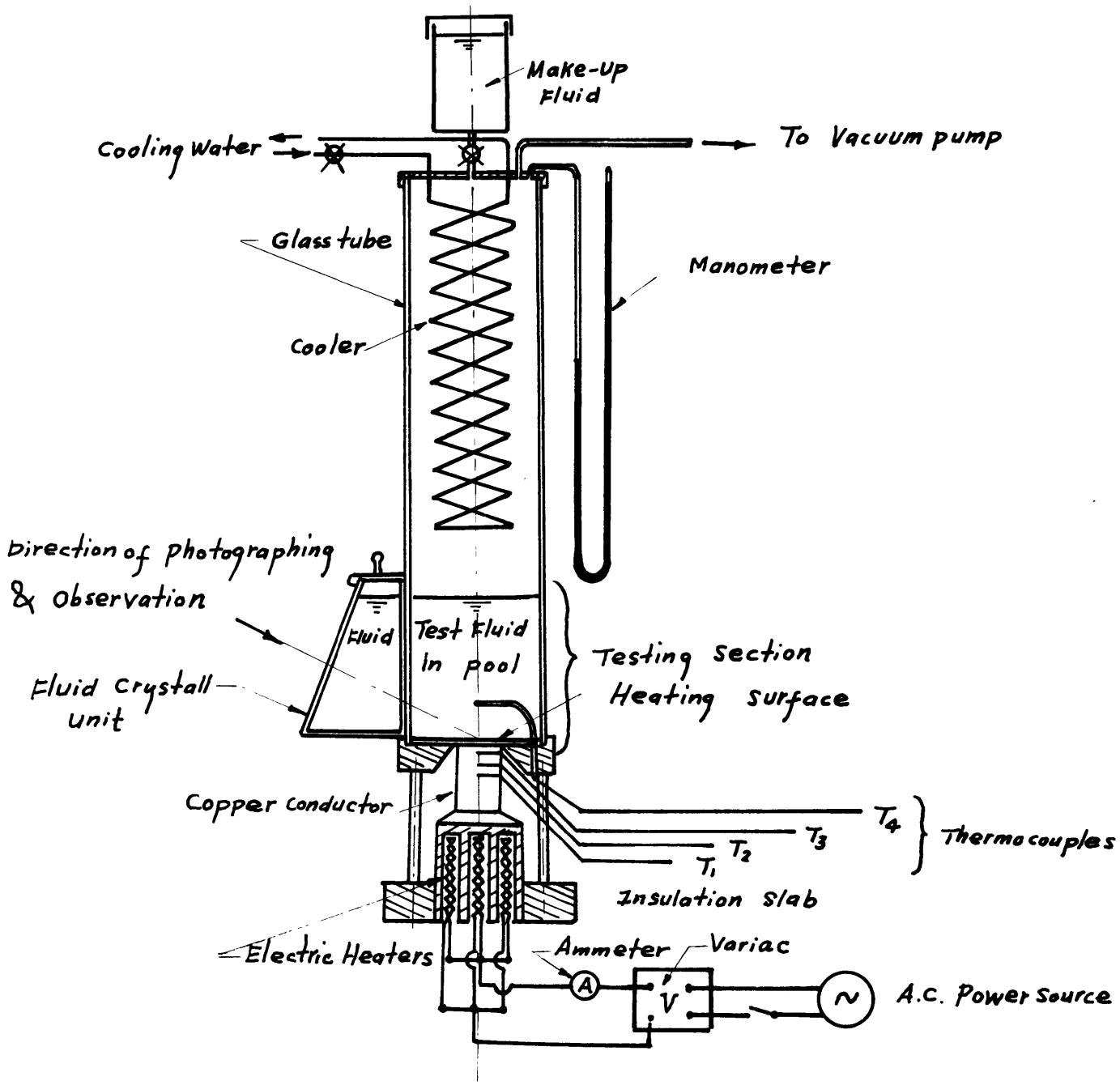

Fig. 29 Pool Boiling Apparatus

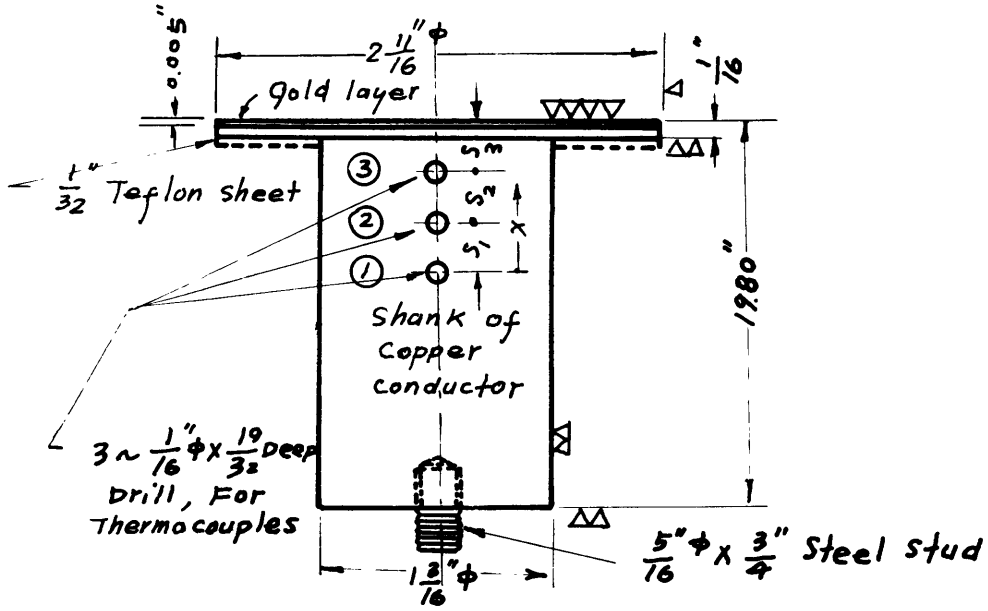

Fig. 30 Detail of Heating Surface and Heat Conductor Shank

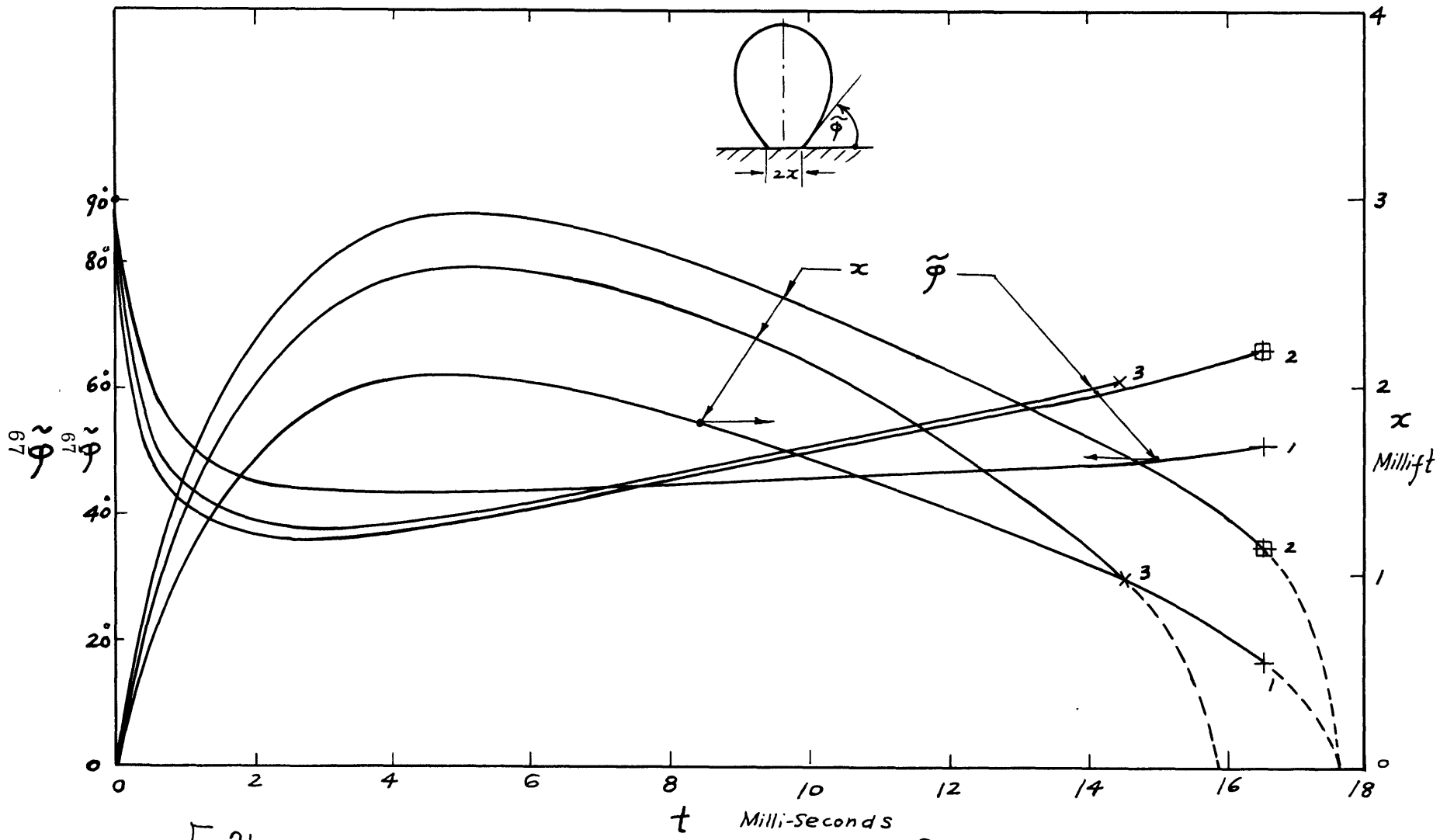

Fig.31 The Dynamical Contact circle radius & the Contact Angle

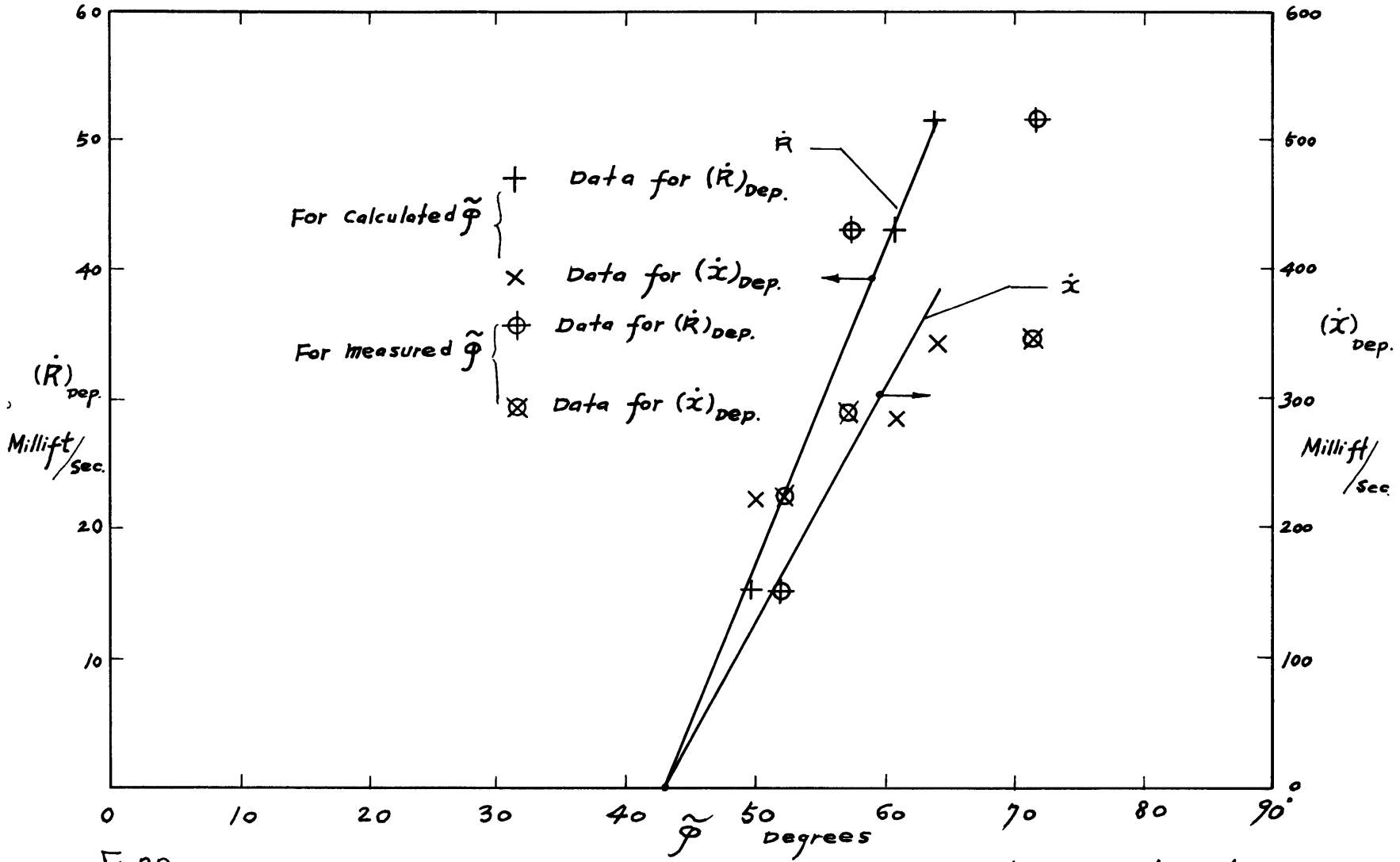

Fig32. The Dynamical Effect of Bubble growth rate to contact angle.

APPENDIX

THE EFFECT OF VELOCITY ON CONTACT ANGLE

It is evident from Figures 12, 13, and 14, that the contact angle is smallest when the contact ring is growing most rapidly and largest when the contact ring is contracting most rapidly. The data reported here are too skimpy to get much of a measure of the importance of this effect, so the purpose of this appendix is to relate the deviations in contact angle from the static condition to the growth velocity of the bubble which is a known quantity. The extensive data of Staniszewski will then be used to determine the best value for the constant in the relationship between these two quantities.

The relationship between the apparent contact angle and contact ring radius is shown in Figure 31 for the three bubbles illustrated in Figures 12, 13, and 14. For these three bubbles, the data of Figure 31 for the rate of contact ring radius change can be obtained at the point of departure along with the associated contact angle. These points are plotted on Figure 32 as three circled crosses. At the same time, the growth rate of the bubbles at departure can be plotted versus the contact angle. These points are the circled X's. There is obviously a similar relationship between these two velocities and the contact angle deviations. As the growth velocity is a known quantity in this work, it is this quantity which has been used to correlate rather than contact ring velocity.

To repeat, the physical velocity of significance in determing contact angle deviations is the contact ring velocity. This, in general, is not known but bears a casual relationship to the growth velocity, so

it is this quantity used to correlate the contact angle deviations. The constant in the equation relating the static contact angle to the dynamic contact angel equation (64) is determined from the extensive data of Staniszewski. Figure 32 gives the calculated and observed values of all these quantities.

NOMENCLATURE

Dimensions in H, M, L, T, θ; The Heat Energy, Mass, Length, Time, and Temperature.

A	Area of heating surface	$[L^2]$
D	Surface characteristic length for natural convection	[L]
K	Thermal conductivity of fluid	$[HT^{-1}L^{-1}\theta^{-1}]$
K_c	Thermal conductivity of copper	$[HT^{-1}L^{-1}\theta^{-1}]$
L	Latent heat of evaporation of fluid	$[HM^{-1}]$
M_1	Inertia mass of fluid surrounding a bubble	[M]
N	Total number of nucleate centerson heating surface	[O]
N_a	Total number of active nucleate centers on heating surface	[O]
N_i	Total number of initiated nucleate centers on heating surface	[O]
P	Pressure in the fluid outside the bubble	$[ML^{-1}T^{-2}]$
Q_R	Heat flux received by heating surface	$[HT^{-1}]$
Q_P	Heat flux predicted by theory	$[HT^{-1}]$
R	Radius of bubble	[L]
R_c	Radius of cavity	[L]
R_d	Departure radius of bubble	[L]
$\tilde{R}$	Meridian curvature radius of bubble at the base circle	[L]
S	Bubble surface	$[L^2]$
T	Temperature	$[\theta]$
T_b	Temperature of vapor in the bubble	$[\theta]$
T_{sat}	Saturation temperature of fluid at system pressure	$[\theta]$
T_w	Wall Temperature	$[\theta]$
T_∞	Temperature of main body of fluid	$[\theta]$
U	Rising velocity of a solid sphere	$[LT^{-1}]$
V	Reading of thermocouple	[Milli volts]

a	Radius of a solid sphere	[L]
b	Radius of curvature of bubble at its top	[L]
c	Specific heat of fluid	$[HM^{-1}\theta^{-1}]$
f	Frequency of bubble generation	$[T^{-1}]$
g	Gravity acceleration	$[L\,T^{-2}]$
h	Distance from the center of a solid sphere to the solid plane boundary	[L]
$\tilde{h}$	Coefficient of heat transfer from wall to the fluid	$[HT^{-1}L^{-2}\theta^{-1}]$
$\tilde{h}_v$	Coefficient of heat transfer from wall to Vapor	$[HT^{-1}L^{-2}\theta^{-1}]$
k	Thermal difusivity of fluid	$[L^2T^{-1}]$
n	Number of nucleate centers per unit area	$[L^{-2}]$
n_a	Number of active nucleater center per unit area	$[L^{-2}]$
n_i	Number of initiative nucleater center per unit area	$[L^{-2}]$
p	Pressure inside the bubble	$[ML^{-1}T^{-2}]$
q	Heat flux density	$[HL^{-2}T^{-1}]$
R	Normalized bubble radius	[O]
t	Time	$[\theta]$
t_d	Departure period	$[\theta]$
t_{ub}	Unbinding period	$[\theta]$
t_w	Waiting period	$[\theta]$
x	Distance from the bubble surface to the axis of revolution of bubble; Wall distance	[L]
z	Distance from the plane tangent to the bubble at top paint of bubble to a point on the bubble surface	[L]
$\wedge$	Constant in dynamic contact angle	[O]
Φ	Velocity potential	$[L^2T^{-1}]$
Ψ	Stream line function	$[L^3T^{-1}]$
γ	Volumetric thermal expansion coefficient of fluid	$[\theta^{-1}]$
δ	Thermal layer thickness	
η	Distance from the bubble center to base plane angle	[L]
θ	$T-T_{sat}$; *Angle*	$[\theta]$; [O]
μ	Coefficient of Viscosity	$[MT^{-1}L^{-1}]$
ν	Kinematic Viscosity	$[L^2T^{-1}]$
ρ	Density of fluid	$[ML^{-3}]$
ρ_v	Density of Vapor	$[ML^{-3}]$

σ	Surface tension of fluid	$[M T^{-2}]$
τ	Normalized time variable	[o]
$\mathcal{V}$	Volume of bubble	$[L^3]$
φ	Angle of Contact in Static Condition	[O]
$\tilde{\varphi}$	Dynamic contact angle at the instant of bubble departure	[O]
φ_b	Base factor	[O]
φ_c	Curvature factor	[O]
φ_s	Surface factor	[O]
φ_v	Volume factor	[O]
Nu	Nusselt number	[O]
Ra	Rayleigh number	[O]

Subscripts

Bc	Bulk convection
cp	Close packed condition
d	Departure
Nc	Natural convection
Sat	Saturation
ub	Unbinding
Vc	Vapor convection
w	Wall; Waiting

REFERENCES

1. Rohsenow, W. M., "Notes on Advanced Heat Transfer I & II", 1959 - 1960, M.I.T.

2. Lin, C. C., "Notes on Theoretical Hydromechanics I & II", 1960-1961, M.I.T.

3. Griffith, Peter, "The Role of Surface Conditions in Nucleate Boiling", A.I.C.E., 1959

4. Westwater, J. W., "Things We Don't Know About Boiling Heat Transfer", Dept. of Chemistry and Chemical Engineering, University of Illinois, 1960.

5. Hsu, Yih-Yun, "An Analytical and Experimental Study of Thermal Boundary Layer and Ebullition", NASA, 1961.

6. Clark, T. A., "Pool Boiling in an Accelerating System", ASME 60-HT-22.

7. Moissis, R. and Berenson, P. J., "On the Hydrodynamic Transitions in Nucleate Boiling", M.I.T., 1961.

8. Zuber, Novak, "The Dynamics of Vapor Bubble in Non-Uniform Temperature Fields", International Journal of Heat Transfer, Vol. 2, pp. 88-98, 1961.

9. Fritz, W., "Berechnung des Maximal Volumens Von Dampfblasen", Physikalische Zeitsehrift, Vol. 36, p. 379, 1935.

10. Staniszewski, B. E., "Bubble Growth and Departure in Nucleate Boiling", Technical Report No. 16, 1959, M.I.T.

11. Wark, T. W., "The Significance of Contact Angle in Floatation", Journal of Physical Chemistry 37, p. 623, 1933.

12. Davidson, J. F., "Bubble Formation at an Orifice of Invicid Fluid", Transaction Institution Chemical Engineering, Vol. 38, 1960.

13. Bashforth, Fr. and Adams, F., "Capillary Action", Cambridge, 1883

14. Hildebrand, F. B., "Notes on Numerical Analysis I & II", 1960-1961, M.I.T.

15. National Research Council of the United States of America, International Critical Tables of Numerical Data Physics, Chemistry and Technology", 1929, McGraw-Hill Book Co.

16. Strenge, P. H., Orell, A., and Westwater, J. W., Microscopic Study of Bubble Growth During Nucleate Boiling", University of Illinois, 1961.

17. Corty, C. and Foust, A. S., "Surface Variables in Nucleate Boiling", American Institute of Chemical Engineers, 1953.

18. Scriven, L. E., "On the Dynamics of Phase Growth", Chemical Engineering Science, 1959, Vol. 10, pp. 1-13.